RESPONSE TO REVIEWER 1

First of all, many thanks to Dr. Guillaume Charria for the number of useful comments that will help to significantly improve the quality of the final version of this manuscript. In relation to the specific suggestions:

Regarding comment 1:

In the introduction, close geographical studies can be mentioned (Marmain's papers in Med Sea; Solabarrieta et al., 2014 in Bay of Biscay; ...).

We have added the suggested references in the following paragraphs:

"In addition, the credibility of HF radar data has been previously tested in extensive validation studies, including direct comparisons of HF radar-derived surface currents with moored ADCP's, point-wise current meters or drifters (Graber et al., 1997; Kaplan et al., 2005; Cosoli et al., 2010; **Solabarrieta et al., 2014**)."

"Other emerging uses include the validation of operational ocean forecasting systems or assimilation into numerical coastal circulation models (**Marmain et al., 2014**; Stanev et al., 2015)."

And the references are:

Solabarrieta, L., Rubio, A., Castanedo, S., Medina, R., Charria, G. and Hernández, C.: Surface water circulation patterns in the southeastern Bay of Biscay: New evidences from HF radar data, Continental Shelf Research 74, pp. 60–76, 2014.

Marmain, J., Molcard, A., Forget, P. and Barth, A.: Assimilation of HF radar surface currents to optimize forcing in the North Western Mediterranean sea, Nonlin. Processes Geophys., Vol. 21, pp. 659-675, 2014.

Stanev, E.V., Ziemer, F., Schultz-Stellenfleth, J., Seemann, J., Staneva, J. and Gurgel, K.W.: Blending Surface Currents from HF Radar Observations and Numerical Modelling: Tidal Hindcasts and Forecasts, Journal of Atmospheric and Oceanic Technology, Vol. 32, pp. 256-281, 2015.

Regarding Section 3.2 - p. 1922 / l. 13:

Why in the qualification part, only May to October 2014 has been considered as for the exploration of current fields, the whole year is considered. Please mention some reasons for this choice.

As reflected in section 2.2., verbatim: **"**It should be noted that current and wind records from B1 are only available from 1 May to 31 October 2014". This is the main reason to limit the validation exercise with the moored current meter to that specific 6-month study period. Since the statistical results obtained are significantly good, within tolerance ranges and in accordance with those previously reported in the literature, it seems reasonable to infer that HF radar performance was accurate during the previous period (January-April 2014). Equally, it seems to be also reasonable to expect a consistent radar performance during the last part of the year (November and December 2014) since no breakdown or anomaly in radar site status were detected, neither changes in the surrounding environment which could negatively impact on the precision of the measured antenna beam pattern (APM, implemented in December 2013) and hence, on the quality of HF radar-derived current data.

Furthermore, the results derived from the annual Quality-Control (QC) of diagnostic parameters (section 4.1) supports the fact that the overall performance of the HF radar system and the health of the three radar sites were solid and consistent, as stated in the Conclusions.

The previous statements reinforce why 1-year long of HF radar data has been chosen to explore and describe the main characteristics of the surface current flow in Ebro River Delta. In addition, a selection of an entire annual cycle provides a more comprehensive insight into the oceanographic features of this relevant marine protected area.

Regarding Section 3.2 - p. 1922 / l. 27-28

A filter is applied on the data and then considered for validation. Is it possible to describe or to overview the quality of the unfiltered products? Maybe it does not make sense due to the uncertainty in the measurements but then it has to be clearly mentioned.

Of course it is possible. **Actually, they have already provided in Figure 4**. This Figure shows the statistical results for raw (unfiltered) products, as stated in the corresponding Figure 4 caption:

"Figure 4. (a) Angular position of Ebro Delta HF radar sites respect to B1 buoy location. Angle values are measured counter-clockwise from East, indicating arc limits and buoy direction. (b-d) Correlation (solid line) and RMSE (dashed line) **between unfiltered radial currents estimated by B1 buoy and those measured by three HF radar sites**, SALO (b), ALFA (c), and VINA (d), using calibrated antenna patterns for a 6-month period May-October 2014. Vertical dotted line represents the angular position of B1. Vertical red solid line denotes the angular position of maximum correlation (CORR), which is gathered with the associated RMSE and bearing offset ($\Delta\alpha$) values."

In Lorente et al. (2014) and Lorente et al. (2015), both referenced in the manuscript, raw and low-passed time series were compared for Gibraltar and Galicia HF radar systems, respectively. The main aim was to check if the statistical metrics would improve after removing the high-frequency "tidal noise". If so, the differences buoy-HF radar can be interpreted in terms of random errors and the wind influence on a diurnal time-scale.

In the present work with Ebro Delta HF radar system, the 6-month (May-October 2014) time series of hourly estimations were low-pass filtered not only for the aforementioned reasons but also for a visualization reason: a 6-month raw time series would be too noisy and degree of agreement could not be qualitatively inferred.

Regarding Section 3.3 - p. 1923 / l. 23:

In this sentence we wonder what is the nature of "raw radar time series" but it is explained later in Section 3.3 - p. 1924 / l. 8-9. Is it possible to detail it before?

Of course it is possible. We have modified the indicated sentence in order to clarify the meaning of “raw time series”:

“To this purpose, maps of the Eulerian mean current field have been constructed at monthly time scale from the raw (unfiltered) radar time series on a subsampled grid”

Regarding Section 3.3 - p. 1924 / l. 12

Could you define/quantify the "significant" portion (even if it is detailed later in the paper)?

Since EOFs are purely statistical, each EOF mode’s statistical significance must be evaluated. Several rules of thumb have been previously proposed indicating when an EOF is likely to be subject to large sampling fluctuations. In the present work, error estimates based on temporal decorrelation scales have been calculated according to North et al. (1982):

$$\delta(\lambda_i) = \lambda_i * (2/N)^{\frac{1}{2}}$$

Where δ_i is the eigenvalue for mode i, and N is the number of degrees of freedom determined using a conservative two-day decorrelation time-scale, following Münchow and Chant (2000). If the confidence intervals from the error estimates of any modes overlap, the modes may be non-orthogonal and can not be considered distinct. Such modes are thus excluded from the EOF analysis and then, the first previous modes can be considered to contain “a significant portion of the total variance”, as stated in the manuscript.

Here, only the first three EOF modes are statistically significant according to the mode selection rule and truncation criterion suggested by North et al. (1982). The first, second and third modes are distinct; however, the fourth mode is not since its error bars overlap with those of mode 5 (not shown).

The first three EOF modes cumulatively account for the 46.1% of the variance for the raw (unfiltered) hourly time series of surface currents. Longer convergence rate is observed for higher-order modes since 150 EOF modes are required to reach the 95% cumulative variance threshold. The modes 4 and 5 represent the 3.66% and 3.24% of the variance, respectively. They are so close in terms of explained variance that the respective error bars clearly overlap, and then they must be left out.

To clarify this issue, a small paragraph has been inserted in section 3.3, summarizing the explanation presented above.

Finally, in section 4.3.2 has been also inserted the following explanatory piece of text:

“Since the EOF analysis has been performed on the unfiltered data set containing relevant high-frequency spatiotemporal variability, the first three EOFs cumulatively account only for the 46.1% of the total variance (26.1%, 15.3% and 4.7%, respectively). Only the first three EOF modes are statistically significant according to the mode selection rule and truncation criterion suggested by North et al. (1982). The first, second and third modes are distinct and uncorrelated; however, the fourth mode is not since its error bars overlap with those of mode 5 (not shown). Therefore, higher order modes will not be further addressed here as they represent a combination of unresolved high-frequency motions or noise (Cosoli et al., 2012a).”

Reference:

North, G.R., T.L. Bell, R.F. Cahalan and F.J. Moeng: Sampling errors in the estimation of empirical orthogonal functions, Mon. Wea. Rev. 110, pp. 699-706, 1082.

Münchow, A. and R.J. Chant: Kinematics of inner shelf motions during the summer stratified season off New Jersey, J. Phys, Oceanogr., 30, pp. 247-268, 2000.

Regarding Section 4.1 - p. 1924 / l. 19

For non-expert, would it be possible to detail a bit more in the text, for example, SNR3 (I noticed that it is mentioned in Table 1 but it would helpful to also have it in the text).

Yes, of course it is possible. We have added the following paragraph in the introduction (before section 4.1) to provide a more detailed definition of this parameter:

“One of the radial metrics that offers the most potential benefits as reliability indicator is the Signal-to-Noise Ratio of sea-echo at the monopole (SNR3), since it has been previously proved to be a valid indicator of both radar site status and onset of HF radar system malfunction (Cosoli et al., 2012b; Roarty et al., 2012).”

Regarding Section 4.1 - p. 1925 / l. 3:

Following the same idea, could you shortly develop the "limitations in the MUSIC algorithm"?

In the introduction section, there is already a sentence that provides some details:

“As MUSIC is employed to resolve ocean surface current structure (Schmidt, 1986), limitations in its performance are related to potentially suspect velocity outputs.”

As previously stated by De Paolo and Terril (2007): “For a given range cell and a given Doppler cell (and thus a given radial current velocity), the MUSIC algorithm can produce a maximum of two bearing solutions. Any more bearing in that range cell with the same radial current velocity will be left out, producing a gap where there is no solution. This is an inherent limitation of using MUSIC with the compact antenna design, with the statistics of the gaps depending on the environmental input”. Complementarily, Cosoli et al. (2012) showed that “in the majority of the cases anomalous values were associated with poor SNR values”.

Therefore, low SNR3 values due to either environmental noise or interferences can lead to ambiguities in the estimation of the direction of arrival (DOA) function performed by MUSIC algorithm. Such ambiguities, based on the existence of more than two bearings in a given range cell with the same current velocity, produce gaps in HF radar spatial coverage (as reflected in Figure 3-b).

To clarify this point, we have added the following sentences to the manuscript:

"SNR3 reached extremely low values, leading to a drastic reduction in the radar spatial coverage presumably related to an inherent limitation of MUSIC algorithm, namely, the extraction of a maximum of two bearing solutions for a given range cell and a given radial current velocity. In this context, poor SNR3 values associated with potential interferences or environmental noise can lead to ambiguities in the estimation of the direction of arrival (DOA) function performed by MUSIC algorithm. Such ambiguities, based on the existence of more than two bearing solutions, eventually produce gaps in HF radar spatial coverage since the additional solutions are excluded."

References:

De Paolo, T., and Terrill, E.J.: Skill assessment of resolving ocean surface current structure using compact-antenna-style HF radar and the MUSIC direction-finding algorithm, Journal of Atmospheric and Oceanic Technology, 24: 1277–1300, 2007.

Cosoli, S., Bolzon, G., and Mazzoldi, A.: A Real-Time and Offline Quality Control Methodology for SeaSonde High-Frequency Radar Currents, Journal of Atmospheric and Oceanic Technology, 29, pp. 1313–1328, 2012b.

Regarding Section 4.2 - p. 1926 / l. 28:

The lag between minimum RMSE and correlation is clearly observed. Could you explain why there is this difference between the efficiency in RMSE and correlation?

As previously stated in section 3.2, "In absence of direction-finding errors (DF), maximum CORR and minimum RMSE values should be found over the arc point closest to B1 location. In presence of DF, the bearing offset is thus expressed as the angular difference between the arc point with maximum correlation and the buoy location."

Since the HF radar system is not completely perfect, we have found small direction-finding errors in each radar site (Figure 4), rated at lower than 8^{o}. Although such errors are small and in accordance with the typical values previously reported (Emery et al., 2004; Paduan et al., 2006), they impacted slightly on the relative position between the maximum correlation and the minimum RMSE, explaining the observed lag. In absence of DF, no lag would be found.

By overall consensus, the bearing offset is defined as the angular difference between the maximum correlation and the buoy location, although other criterion could have been used, i.e., the angular distance between the minimum RMSE and the buoy location. We chose the first option to follow the worldwide accepted methodology.

Section 4.2 - p. 1928 / l. 21-24:

For the Taylor diagram (Fig. 7), results will be clearer to read and to interpret if you consider using the normalised (in standard deviation) version of the diagram. Examples are available in Taylor (2001) in Figure 5 or Figure 8.

According to our own experience with model data comparisons, normalized pattern statistics are significantly clearer and easier to interpret especially when trying to summarize on a single Taylor diagram a variety of fields (i.e., temperature, salinity, surface currents, etc.). Since the units of measure are different, statistics benefit from the fact of being nondimensionalized, leading to a more simplified graph.

However, we modestly consider that this is not the case. As only one type of field has been considered (HF radar-derived surface currents), we honestly think that the Taylor diagrams used in the present study are more appropriate because information relative to the monthly variability of measurements (standard deviation) and the monthly mismatch radar-buoy (RMSE) are clearly exposed. In the case of normalized Taylor diagrams, RMSE values disappear and the standard deviation of the reference is always plotted at unit distance from the origin, resulting in an excessively plain diagram where only correlation coefficients remain unchanged. In this context, we would like to show all the statistical information obtained.

Section 4.2 - p. 1929 / l. 21-25: In spectra, how do you explain a larger energy in high frequency (mainly CW spectra) in HF radars as the buoy has most probably an higher sampling frequency?

Both instruments employed in this work (HF radar and current meter) provide quality-controlled hourly averaged current velocity vectors. Therefore, there is no difference in terms of sample frequency. However, the current meter measures at a nominal depth of three meters, whereas HF radar derived maps are representative of current velocities in the upper first meter of the water column. In this context, it seems reasonable to suspect that radar estimations are influenced by energetic high-frequency processes related to air-sea interaction like highly variable and strong wind gusts, which are not contained in sub-surface current estimations provided by the current meter.

To clarify this point, a brief comment has been added to the new version of the manuscript:

“Finally, a drop of energy and later flattening about 2 cpd are common for the CW components of both B1 and radar spectra, although the latter presents larger energy at that frequency band. Radar surface estimations are influenced by energetic high-frequency processes related to air-sea interaction like highly variable and strong wind gusts, which are not fully contained in sub-surface current estimations provided by the current meter.”

Section 5 - p. 1935 / l. 22: In my opinion, numerical models provide a "quantitative" picture of the 3D dynamics.

Since we fully agree with this comment, “qualitative” has been replaced by “quantitative”.

As a general comment, it would be useful to have the three timelines of the measurements to see gaps in the time series.

This useful suggestion has been taken into account: a specific section (section-c) has been added to Figure 1 to illustrate the continuity of the records (from HF radar sites and B1 buoy) employed in the present study.

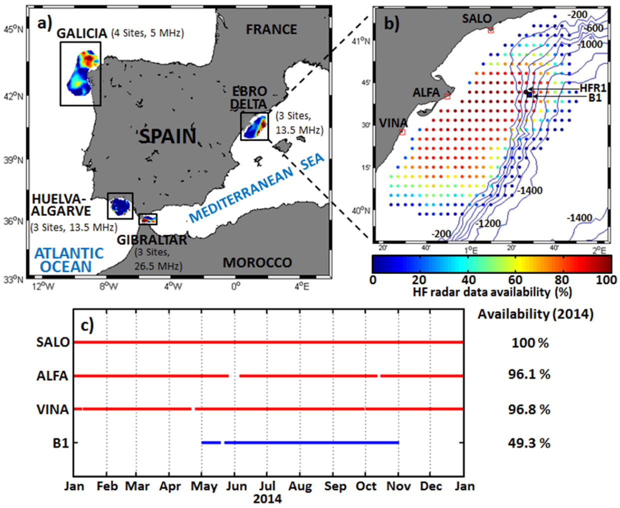

Figure 1. (a) HF coastal radar network currently operated by Puertos del Estado (b) HF radar deployed at the Ebro Delta, composed by three sites: Salou (SALO), Alfacada (ALFA) and Vinaroz (VINA). Colored dots denote the temporal coverage in percent of HF radar surface current total vectors for the entire year 2014. Isobath depths are labeled every 200 m. Location of Tarragona buoy (B1) is marked with filled blue squares. HFR1 denotes the radar grid point closest to B1 position. (c) Time lines of HF radar sites (red) and B1 buoy (blue) current data availability for 2014.

— Technical corrections —

In Abstract: My Ocean IBI - IBI acronym to be detailed.

The sentence has been replaced by:

"Future works should include the use of verified HF radar data for the rigorous skill assessment of operational ocean circulation systems currently running in Ebro estuarine region **like IBI (Iberia–Biscay–Ireland) regional system**, implemented within the frame of MyOcean projects and the Copernicus Marine Environmental Monitoring Service (CMEMS)."

Figure 1: HFR1 and B1 not visible

Figure 1 has been replaced by a new one with the aim of highlighting HFR1 and B1 locations and solving the reported issue (see Figure 1, above)

p. 1941: belowlisted => below listed

Done!

p. 1941: Diagnose => Diagnosed

Done!

RESPONSE TO REVIEWER 2

Many thanks to the anonymous reviewer for taking her/his time to read the manuscript and also for sharing her/his point of view in the Open Discussion Forum. In relation to the specific suggestions:

This work presents a quality control methodology for HF radars applied to observations in the area of Ebro Delta. This is a useful study, which could be beneficial for future use of HF radar data. However the paper is too long; it presents a lot of well-known details of HF radars from other papers. It has to be substantially shortened, particularly the first part.

The new version of the manuscript has been shortened in order to fulfil reviewer2's request, trying to avoid redundant information presented in sections 1, 3 and 5. Some explanatory paragraphs and the bibliographic references shown in the introduction have been kept to provide a basic background for non-expert readers.

Furthermore, the geophysical relevance is not well explored and the presentation is sometimes misleading (difficult to differentiate between what authors and others have done).

Some modifications have been carried out in order to strengthen the discussion of results and to better explore the geophysical relevance of this study. For instance, according to reviewer3's recommendation, Figure 12 has been added with the aim of investigating the relative contribution of local wind as forcing mechanism. Particular emphasis has been placed to explore the link with the principal component of the second EOF mode of HF radar surface currents (depicted in Fig. 10-c).

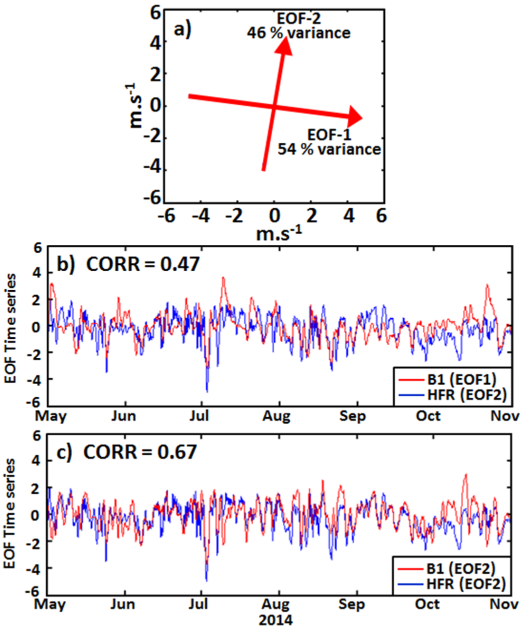

Figure 12-a shows wind principal axes as derived from 6-month (May-October 2014) wind data measured by B1 buoy. Figure 12-b presents the principal components of the first EOF mode from B1 wind (red) and the second EOF mode of CODAR currents (blue), filtered with a 1-day moving mean. The amplitudes are normalized by their respective standard deviations. Equally, Figure 12-c shows the principal components of the second EOF mode from B1 wind (red) and the second EOF mode of CODAR currents (blue). As reflected from the associated correlation coefficients (0.47 and 0.67, respectively), the degree of agreement of the principal components is significant. This underlines the close relationship between HF radar mode-2 variability and the variability of local wind.

Regarding the presentation, the authors have modified several sections of the article with the aim of avoiding any confusion about what has been achieved in this paper and what has been previously done.

Specific comments:

Caption Fig. 2. Please don’t repeat here what you say in text.

Ok. Redundant information has been removed from Figure 2 caption.

The presentation of section 4.2, as it is now, is too technical. Much of what is shown in this section can be considered as the same information presented in a different way. I wonder if Taylor diagram is not sufficient to explain most of what has been found. Perhaps the rest can be briefly summarized in text.

The section 4.2 focuses on the validation of radar measurements with independent in situ observations by means of the evaluation of direction-finding capabilities and the angular distribution of radial velocity uncertainties. This approach has been previously adopted by a vast number of previous research works published in scientific journals (Emery et al., 2004;

Paduan et al., 2006; Cosoli et al., 2010; Liu et al., 2014), not only on technical reports. Therefore, we honestly consider this section is not too technical and it suits the scope of the Special Issue. The information provided in Figures 4-7 is not redundant but relevant and complementary, as it is shown:

Figure 4, related to validation of **radial vectors**, focuses on bearing offset determination and directional accuracy.

Figure 5, related to validation of **radial vectors**, shows the degree of agreement between radar-derived and current meter radial vectors, for the radar arc point closest to B1 buoy location.

Figure 6, related to validation of **low-pass filtered total vectors**, reflects the concordance between radar-derived and current meter total vectors, for the radar regular grid point closest to B1 buoy location and for a 6-month period (May-October 2014). In addition, monthly averaged values for both instruments are presented with the aim of characterizing the basic features (**at sub-inertial temporal scale**) of the shelf-slope jet flowing southwestwards.

Figure 7, related to validation of **unfiltered total vectors**, analyses HF radar performance and accuracy on a monthly basis in order to check the consistency and robustness of radar data.

Since the other two reviewers have not pointed out any drawback or deficiency in section 4.2, we honestly consider that it should remain as it currently is.

The discussion of results is a complex mixture of results from other authors and present study. One example is in p. 1930 "The jet is intensified in October as a result of the increase of the mesoscale activity (Font et al., 1995), reaching ultimately a peak strength in December". I would suggest that you tell "your story" as seen in your results and then say what agrees and disagrees with previous studies. More important is however to say what is the new finding originating from this new data set. Section 4.3.2 You say "The buoyancy input introduced by large estuarine outflows, together with topographic effects, lead to the development of the aforementioned anticyclonic coastal eddy on the southern side of the delta." Can you decipher this from the HFR observations? Please, concentrate your presentation on what you find in your observations and tell us what new we learn from them.

Before the referenced sentence in section 4.3.2, the following paragraph can be found in section 4.3.1:

"A coastal anticyclonic eddy can also be observed in radar data, confined south of Ebro Delta mouth (Fig. 9 – a, b, c). This well-documented hydrodynamic feature is due to the interaction of the buoyancy-driven flow with the topography, reinforcing the shelf/slope front that drives the general circulation to the south-southwest (Font et al., 1990; Salat et al., 2002)."

Firstly, the authors state what can be observed from HF radar data. Then, the finding is confronted with evidences from previous researches focused in the same study area using instrumentation different from HF radar, later providing the reported explanation and referencing those works.

Aligned with the suggestion above (*'tell "our story" and they say what agrees or disagrees with previous studies'*), the paragraph has been rewritten:

"A coastal anticyclonic eddy can also be observed in radar data, confined south of Ebro Delta mouth (Fig. 9 – a, b, c). This hydrodynamic feature has been well-documented in previous studies (Font et al., 1990; Salat et al., 2002), which stated the interaction of the buoyancy-driven flow with the topography as triggering source of the clockwise gyre, eventually reinforcing the shelf/slope front that drives the general circulation to the south-southwest."

"Temporal variation in the strength of these three EOF modes is represented by their corresponding time coefficients". Better use the accepted name for these coefficients.
The aforementioned sentence has been modified accordingly:
"Temporal variation in the strength of these three EOF modes is represented by their corresponding time coefficients (**also called principal components**), shown in Fig. 11."

In this part I wonder what would be the result (% of variance) if you work with filtered data and compare with, say MyOcean/Copernicus product.
Although the radar-model comparison exercise is still underway and perhaps the question is out of scope of the present manuscript, preliminary results indicate a close HF radar-IBI agreement in terms of EOF analysis and variance explained for raw (unfiltered) surface current data. The three dominant modes of variability for Ebro Delta HF radar (IBI model) account for the 46.1% (49.2%) of the variability, with the first mode explaining the 26.1% (26%), the second mode represents the 15.3% (17.2%) and the third mode accounts for the 4.7% (6%).
Regarding the EOF spatial patterns, the first two modes derived from HF radar data and IBI model outputs are pretty similar, with the main differences arising from the third EOF mode: although both introduce complexity to the rather uniform surface patterns described by the first two modes, they do it in distinct ways. In the case of the HF radar, a clear divergence of the flow can be detected in the southernmost part of the spatial domain (Fig. 10-d), whereas IBI-derived mode 3 (not shown) reveals a complete clockwise eddy, with the associated core slightly displaced to the south-west part of the domain.

Because CODAR is not the only HF radar system I wonder whether the proposed methodology is applicable or not applicable to WERA. Lots of literature on some quality control issues for WERA were recently presented by Stanev et al. (2015). I mention this work because error estimates (statistics) are very important for data assimilation, and perhaps you have to mention this useful aspect of your research in your revised manuscript.
The authors are fully aware of the existence of several radar systems on the market, not only CODAR or WERA. The assessment of radar data accuracy and development of quality control (QC) procedures implemented at various stages of data processing are ongoing research areas, regardless of the manufacturer.
In this context, significant efforts are currently underway to identify occasional non-realistic radar current vectors (defined as spikes, spurious values or corrupted data and to implement individual QC index. A considerable number of QC works with WERA systems have been published and are indeed cited in the present manuscript (see below), since they

are perfectly valid for any type of HF radar system, and vice versa: QC methodologies with CODAR systems are also applicable to other kind of radar systems since they rely on fundamentally similar physics and Doppler processing algorithms to infer the range and radial velocity of the scattering surface.

The WERA works referenced in the present article are the following:

Gomez, R., Helzel, T., Petersen, L., Kniephoff, K., Merz, C.R., Liu, Y., and Weisberg, R.H.: Real-time quality control of current velocity data on individual grid cells in WERA HF radar, Oceans 2014, Taipei, pp. 1-7, 2014.

Gomez, R., Helzel, T., Merz, C.R., Liu, Y., Weisberg, R.H., and Thomas, N.: Improvements in ocean surface radar applications through real-time data quality-control, Conference: Current, Waves and Turbulence Measurement (CWTM), IEEE/OES, Florida, USA, March 2015.

Liu, Y., Weisberg, R.H., and Merz, C.R.: Assessment of CODAR SeaSonde and WERA HF Radars in Mapping Surface Currents on the West Florida Shelf, Journal of Atmospheric and Oceanic Technology, 31, 1363–1382, 2014.

Wyatt, L.: Improving the quality control and accuracy of HF radar currents, IEEE Oceans 2015, Genova, pp. 1-9, 2015.

Stanev, E.V., Ziemer, F., Schultz-Stellenfleth, J., Seemann, J., Staneva, J. and Gurgel, K.W.: Blending Surface Currents from HF Radar Observations and Numerical Modelling: Tidal Hindcasts and Forecasts, Journal of Atmospheric and Oceanic Technology, Vol. 32, pp. 256-281, 2015.

As it can be seen, Stanev et al. (2015) has been included in the reference section, and the following sentence added to the Introduction:

"Other emerging uses include the validation of operational ocean forecasting systems or assimilation into numerical coastal circulation models (Marmain et al., 2014; Stanev et al., 2015)."

Page 1914, Line 10: "The main goal of this work is to present a combined QC methodology for the specific case of Ebro HF radar (although easily expandable to the rest of PdE radar systems)". Related to the previous comment, I wonder how applicable the method is to tidally-dominated environments.

As previously mentioned, this QC methodology is applicable to any HF radar system, regardless of the manufactures and/or the environment, since they all rely on fundamentally similar physics and Doppler processing algorithms to infer the range and radial velocity of the scattering surface. Actually, this approach has been applied to the four HF radar systems operated by Puertos del Estado (see Figure 1-a), included the network deployed in Galicia (NW Spain, a tidally-dominated region) or the network deployed in the Strait of Gibraltar, where the most important sources of transport variability are the diurnal and semi-diurnal constituents. The four HF radar systems are routinely monitored on the dedicated website mentioned in the manuscript.

Page 1919, Line 20: “representative of current velocities in the upper first meter of the water column”. Please specify under which conditions this 1m is valid.

HF radar data are representative of a certain depth of the water column. Such depth is related to the nominal radar frequency at which HF radar system operates and also to ocean wavelength. As reflected in the attached CODAR Table (below), the significant wave height at which second order spectra saturates the first order and no current measurements possible is 13 metres, for the specific case of Ebro delta HF radar system (13.5 MHz).

SeaSonde Operational Performance vs. Frequency

Radar Frequency (MHz)	Radar Wavelength (m)	Ocean Wavelength (m)	Ocean Wave Period (s)	Depth of Current[1] (m)	Typical Range[2] (km)	Typical Resolution[3] (km)	Typical Bandwidth (kHz)	Upper $H_{1/3}$ Limit[4] (m)
5	60	30	4.5	2	175-220	6-12	15-30	25
12	25	12.5	2.5	1-1.5	60-75	2-5	25-100	13
25	12.5	6	2	.5-1	35-50	1-3	50-300	7
48	6	3	1.5	<.5	15-20	.25-1	150-600	3

1. Depth averaged current
2. Range based on 40W avg power output. Salinity, wave climate and RF noise may affect this.
3. Based on bandwidth approval only - no system limitations - higher resolution will cause some range loss
4. Significant Waveheight at which 2nd order spectra saturates 1st order and no current measurements possible

Page 1920, Line 20: “current velocity vectors at a nominal depth of three meters” How well this combines with 1m mentioned above?

In section 4.2, the following piece of text can be found:

“**Instrument-to-instrument comparisons present intrinsic limitations since both devices operate differently and at distinct nominal depths. A fraction of observed radar-B1 differences can thus be explained in terms of different sampling strategies on disparate time and space scales (Ohlmann et al., 2007)**. In this context, many of the uncertainties associated with HF radar technology are geometric in nature. Apart from the instrumental noise, other sources of potential errors in vector currents might be the sub-grid horizontal shear**, the geophysical variability within the water column** (Graber et al, 1997) and some specific processes, namely, the Stokes drift, the Ekman drift and baroclinity (Paduan et al., 2006).”

Therefore, the differences observed between HF radar data and point-wise current meter observations must be carefully interpreted since the vertical shear resulting from seasonal stratification might play a significant role during the validation exercise. No additional changes have been introduced in the paper since we consider this point has been clearly exposed.

Section 3.3 can be substantially shortened and integrated with Section 4.

We are afraid that there is a conflict between this suggestion and both reviewer1 and Dr. Cosoli's recommendation:

"An interesting EOF analysis is presented, with the complex-valued approach, though some authors suggest using the real-valued approach. They are presented as statistically significant- **<u>however no information is given on the confidence levels or on the degrees of freedom to support this statement</u>**"

The following paragraphs have been inserted in section 3.3 in order to provide further details about the significance of the three EOF modes selected in the present study:

"Since EOFs are purely statistical, each EOF mode's statistical significance must be evaluated. Several rules of thumb have been previously proposed indicating when an EOF is likely to be subject to large sampling fluctuations. In the present work, error estimates based on temporal decorrelation scales have been calculated according to North et al. (1982):

$$\delta(\lambda_i) = \lambda_i * (2/N)^{\frac{1}{2}}$$

Where δ_i is the eigenvalue for mode i, and N is the number of degrees of freedom determined using a conservative two-day decorrelation time-scale, following Münchow and Chant (2000). If the confidence intervals from the error estimates of any modes overlap, the modes may be non-orthogonal and can not be considered distinct and uncorrelated. Such modes are thus excluded from the EOF analysis and hence only the first previous modes can be considered to contain a significant portion of the total variance and to properly reproduce the observed surface current fields."

Literature

E. V. Stanev, F. Ziemer, J. Schulz-Stellenfleth, J. Seemann, J. Staneva, and K.-W. Gurgel, 2015: Blending Surface Currents from HF Radar Observations and Numerical Modeling: Tidal Hindcasts and Forecasts. J. Atmos. Oceanic Technol., 32, 256–281.

As previously mentioned, this work has been included in the reference section and the following sentence added to the Introduction:

"Other emerging uses include the validation of operational ocean forecasting systems or assimilation into numerical coastal circulation models (Marmain et al., 2014; Stanev et al., 2015)."

RESPONSE TO REVIEWER 3

Many thanks to Dr. Jeffrey Paduan for the number of useful comments that will help to significantly improve the quality of the final version of this manuscript. In relation to the specific suggestions:

The manuscript by Lorente et al. is focused on the performance of a network of high frequency (HF) radar systems deployed along the eastern coast of Spain. Data from three radar sites for a full year in 2014 are analyzed. HF radar observations of ocean surface currents are increasingly important components of ocean observing systems. Descriptions of these observations in new regions over long time frames are of interest both to the local scientists and marine resource managers and to other users of HF radar systems. As the data set here is extensive and the analyses and interpretations reasonable, I recommend the manuscript for publication.

The manuscript could, of course, be improved in a few areas. Although the background sections are thorough and well cited, they also have a good deal of redundant information with the data sections. Whole paragraphs are repeated in the two sections (and in some cases again in the summary and concluding remarks section). The introduction and/or data sections should be shorted.

Section 5 (Summary and concluding remarks) has been renamed to “Concluding remarks and future work”. Accordingly, the section has been substantially shortened with the aim of avoiding redundancy with information already provided in previous sections.
Equally, sections 1 and 3 have been thoroughly revised and compacted by deleting any repeated expressions.

In several places within the text as well as in the title, the authors suggest that the main point of the manuscript is to describe some new type of quality control for HF radar observations. I think that this is misleading as the manuscript really is a balanced look at the performance of the particular HF radar network using previously described methods. The authors highlight the variability over the 12-month record of radar-specific parameters, such as the signal-to-noise ratio (SNR) on the monopole receive antenna elements. The study does not, however, utilize these quality indices on a point-by-point basis. Neither does it show through any type of comparison that use of the SNR-based quality metrics can improve the results. Because of this, I recommend a change in the title and a diminished focus on quality control.

With the aim of reducing the focus on quality control and placing more emphasis on the characterization of the surface circulation with HF radar data, the title has been changed to “Evaluating the surface circulation in Ebro Delta (NE Spain) with quality controlled High Frequency radar measurements”. For consistency reasons and homogeneity, several sections (abstract, introduction and concluding remarks) have been modified in order to remark this alternative perspective.

The discussion of EOF results would be strengthened if a local wind time series were added to the EOF mode time series shown in Figure 11. Is the mode-2 variability really correlated with variability of the Mistral wind?

A new figure (Fig. 12) has been added to the manuscript (attached below) with the purpose of investigating the relative contribution of local wind as forcing mechanism. Particular emphasis has been placed to explore the relationship with the principal component of the second EOF mode of HF radar surface currents (depicted in Fig. 10-c). To this aim, an EOF analysis of hourly wind measurements provided by B1 buoy for a 6-month period (May-October 2014) is provided.

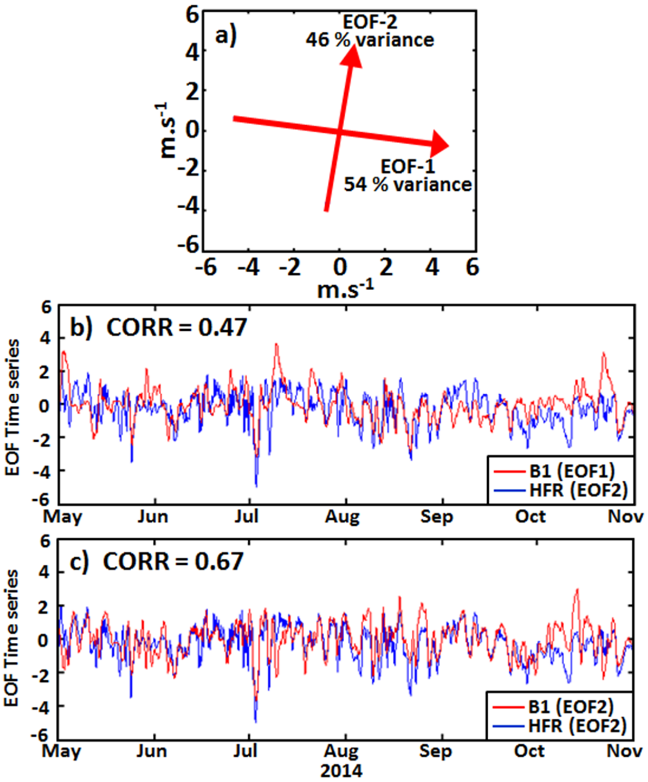

Figure 12-a shows wind principal axes as derived from hourly wind data, measured at a nominal height of 3 metres by B1 buoy, which has a wind speed and direction sensor manufactured by R. M. Young Company. Figure 12-b presents the principal components of the first EOF mode from B1 wind (red) and the second EOF mode of CODAR currents

(blue), filtered with a 1-day moving mean. The amplitudes are normalized by their respective standard deviations. Equally, Figure 12-c shows the principal components of the second EOF mode from B1 wind (red) and the second EOF mode of CODAR currents (blue). As reflected from the associated correlation coefficients (0.47 and 0.67, respectively), the degree of agreement of the principal components is significant.

Regarding the following sentence in section 4 of the manuscript:

"The second EOF (Fig. 10 - c) shows a homogeneous spatial structure, perpendicular to the first mode, with a well-defined offshore-directed flow presumably driven by persistent and intense (up to 100 km/h) northwesterly winds (called 'mistral winds') channeled by the narrow Ebro Valley (Font, 1990)."

The authors firstly hypothesized the northwesterly Mistral wind to be the main forcing mechanism for the offshore-directed flow since it is very energetic and dominant during the cold season (October-May). According to the results depicted in Fig. 12, Mistral winds play a relevant, but secondary role compared to south-southwesterly winds.

Accordingly, the aforementioned sentence has been modified:

"The second EOF (Fig. 10 - c) shows a homogeneous spatial structure, perpendicular to the first mode, with a well-defined offshore-directed flow"

To provide further details about the influence of local wind forcing, the following piece of text has been added to section 4.3.2:

"In order to define the prevalent wind directions registered at B1, the major and minor variance axes have been determined (Fig. 12 - a). The results show that the main variability occurs along a direction 99º azimuth containing the 54% of the total energy. This is the EOF1 mode, largely aligned with persistent and intense northwesterly mistral winds channeled by the narrow Ebro Valley (Font, 1990). The orthogonal EOF2 is oriented 9º clockwise from north and holds the remaining 46% of the variance, capturing mainly the influence of alongshore winds.

Linear correlation coefficients have been computed between the principal components related to the two main wind EOF modes of variability and radar-derived EOF2, since the cross-shelf circulation shown in Fig. 10-c might be presumably driven by strong local winds. The high correlation between the filtered principal components can be readily seen in Fig. 12 (b-c), with a value of 0.47 (0.67) for wind-PC1 (PC2) and radar-PC2, respectively. The results underline that the surface current variability in Ebro Delta can be influenced by wind action, in accordance with Espino et al. (1998), who demonstrated such relationship when winds are strong and steady enough. The higher agreement between both wind-radar PC2 appears to be consistent with Ekman transport to the right of the wind direction. By contrast, northwesterly mistral wind events (PC1) are expected to enforce the prevalent offshore-directed circulation regime (radar EOF2) by increasing the mean speed of the flow.

Equally, the influence of local wind forcing on HF radar EOF1 mode has been assessed (but not shown), with a correlation coefficient of 0.52 (-0.28) for wind PC1 (PC2). This finding highlights the impact of mistral winds on the predominant southwestward flow, by inducing an Ekman veering."

Regarding minor Comments:

Page 3, Line 3: "jet which" should be "jet, which"
Page 3, Line 10: "dynamic" should be "dynamics"
Page 3, Line 19: "a 13.5 MHz" should be "a network of 13.5 MHz" and Line 20: "radar able" should be "radar systems able"
Page 4, Line 11: "failure problems" should be "failures"
Page 8, Line 11: "measurements accuracy" should be "measurement accuracy"

All the suggested minor modifications have been properly addressed in the new version of the manuscript.

~~A combined Quality-Control methodology in Ebro Delta (NE Spain) High Frequency radar system~~

Evaluating the surface circulation in Ebro Delta (NE Spain) with quality-controlled High Frequency radar measurements

P. Lorente[1], S. Piedracoba[2], J. Soto-Navarro[1] and E. Alvarez-Fanjul[1]

[1]{Puertos del Estado, Avenida del Partenón 10, 28042, Madrid, Spain}

[2]{University of Vigo, Marcosende s/n, 36310, Vigo, Pontevedra, Spain}

Correspondence to: P. Lorente (plorente@puertos.es)

Abstract

Ebro River Delta is a relevant marine protected area in the western Mediterranean. In order to promote the conservation of its ecosystem and support operational decision making in this sensitive area, a three site standard-range (13.5 MHz) CODAR SeaSonde High Frequency (HF) radar was deployed in December 2013. The main goal of this work is to explore basic features of the sea surface circulation in Ebro estuary as derived from reliable HF radar surface current measurements. To this aim, a a combined quality control methodology was applied: ~~Since there is a growing demand for reliable HF radar surface current measurements, the main goal of this work is to present a combined quality control methodology. Firstly,~~ firstly one year-long (2014) real-time web monitoring of nonvelocity-based diagnostic parameters wa~~i~~s conducted ~~in order~~ to infer both radar site status and HF radar system performance. Signal-to-noise ratio at the monopole exhibited a consistent monthly evolution although some abrupt decreases (below 10 dB), occasionally detected in June for one of the radar sites, impacted negatively on the spatiotemporal coverage of total current vectors. It seemed to be sporadic episodes since radar site overall performance was found to be robust during 2014. Secondly, a validation of HF radar data with independent *in situ* observations from a moored current meter was attempted for May-October 2014. The accuracy assessment of radial and total vectors revealed a consistently high agreement. The directional accuracy of the HF radar was rated at better than 8º. The correlation coefficient and RMSE values emerged in the ranges [0.58-0.83] and [4.02-18.31] $cm \cdot s^{-1}$, respectively. The analysis of the monthly averaged current maps for 2014 showed that the HF radar properly represented basic oceanographic features previously reported, namely: the predominant southwestward flow, the coastal clockwise eddy confined south of Ebro Delta mouth or the Ebro River impulsive-type freshwater discharge. The EOF analysis related the flow response to local wind forcing and confirmed that the surface current field evolved in space and time according to three significantly dominant

modes of variability.~~Future works should include the use of verified HF radar data for the rigorous skill assessment of operational ocean circulation systems currently running in Ebro estuarine region like MyOcean IBI.~~

1. Introduction.

The circulation in Ebro continental margin (NE Spain, Fig. 1 - a) is mainly thermohaline and characterized by a quasi-permanent barotropic shelf-slope jet which flows southwestwards, 'the North current', only altered by clockwise inertial oscillations and some short periods of current reversals. This relatively low-intensity current flow (10 $cm \cdot s^{-1}$) is in geostrophic balance with the so-called Catalan front, which is a permanent density front associated with strong salinity gradients maintained by the Ebro River runoff (Font *et al*., 1988a).

The marine circulation near the delta, although dominated by the alongshore large-scale dynamic, presents a complex structure strongly influenced by the topography, the seasonality of the remarkable Ebro River discharges (Font *et al*., 1988b), the changing wind conditions and the water column thermal stratification (Salat *et al*., 2002). Nonetheless, the tidal influence in the continental shelf currents field is very weak as expected for a microtidal and low-energy environment (Jimenez *et al*., 2002).

Since the Ebro River Delta is one of the most relevant marine protected areas in the western Mediterranean in terms of biodiversity, an important monitoring activity is performed to manage this deltaic coastal region and promote the conservation of its ecosystem. In order to support marine domain awareness and operational decision making in this sensitive area, a network of ~~-~~13.5 MHz CODAR SeaSonde High Frequency (HF) radar systems has been deployed (Fig. 1 - b). HF radar has been steadily gaining recognition as an efficient land-based remote sensing instrument for mapping surface currents at high spatial and temporal resolutions in near real time~~, able to monitor the spatiotemporal evolution of the surface current fields in near real-time, has been deployed (Fig. 1 - b).~~ This ~~shore-based remote-sensing~~ technology presents a broad range of practical applications, encompassing management (SAR operations, oil spill emergencies), commercial (vessel tracking, ocean energy production) and research (ecology, water quality, fisheries) uses. Other emerging uses include the validation of operational ocean forecasting systems or assimilation into numerical coastal circulation models (Marmain et al., 2014; Stanev et al., 2015).

As a consequence, there is a growing demand for quality-controlled ~~reliable and accurate~~ HF radar surface current measurements. Since HF radar estimations are subject to many potential uncertainties (namely: power-line disturbances, radio frequency interferences, ionosphere clutter, ship echoes, antenna pattern distortions or environmental noise - see Kohut and Glenn, 2003), ~~radar status and performance must be routinely examined by means of the development of quality check procedures and the execution of continuous validation works with independent *in situ* instruments.~~

~~The development of quality control (QC) procedures, implemented at various stages of data processing, constitutes an ongoing research area. A dedicated web interface has been developed to operationally monitor in real time the evolution of a variety of nonvelocity-based diagnostic parameters provided by the manufacturer (CODAR Ocean Sensors -COS-)~~

Con formato: Ajustar espacio entre texto latino y asiático, Ajustar espacio entre texto asiático y números and listed in Table 1. Such parameters are used as indicators of HF radar system integrity and health (Roarty *et al*., 2012; Emery and Washburn, 2007) since anomalous values, inconsistencies or sharp fluctuations might be related to quality degradation, potential malfunctions, or even failure problems, triggering alerts for troubleshooting.

Mmany efforts have been recently devoted to identify occasional non-realistic radar current vectors. Such artefacts (defined as spikes, spurious values or corrupted data) are, generally detected at the outer edges of the radar domain and flagged in accordance with a pre-defined protocol. An individual QC index, based on an integer number derived from a battery of tests, should be assigned for each and every single radar grid-cell to indicate the quality level of each measured value (Gomez *et al*., 2015).

Con formato: Sangría: Primera línea: 0 cm

The artefacts (defined as spikes, spurious values or corrupted data) can be subsequently eliminated from the data stream in real time (Cosoli *et al*., 2012b) or offline (Liu *et al*, 2014). Other approaches are focused, in addition, on replacing noisy values with more reliable estimates (Wyatt *et al*., 2015) by using open-boundary model analysis (Kaplan and Lekien, 2007) or statistical mapping (Barrick *et al*., 2012). However, the main drawback lies with the potential removal of accurate data when the discriminating algorithm is based on tight thresholds. Some fine-tuning, based on the specific local conditions of the system, is thus required to have the right trade-off between confirmed outlier identification and false alarm rate, maximizing the benefit of the applications of these methods (Gomez *et al*., 2014).

Whereas some quality indexes are assigned according to velocity-based QC schemes, other approaches intend to use nonvelocity-based metrics related to the characteristics of the received signal in order to implement advanced quality controls and reduce the systematic errors in radar current estimates (Kirincich et al., 2002). One of the radial metrics that offers the most potential benefits as reliability indicator is the Signal-to-Noise Ratio at the monopole (SNR3), since it has been previously proved to be a valid proxy for radar data quality both radar site status and onset of HF radar system malfunction (Cosoli *et al*., 2012b; Roarty et al., 2012). Complementarily, a big jump in the average state over time in antenna parameters (*e.g*. amplitude corrections for loops 1 and 2 to the monopole, AMP1 and AMP2, respectively) may indicate an antenna problem and should be investigated (COS, 2005).

In this context, a number of previous works have focused on defining optimum threshold levels since there is still no worldwide consensus (Kirincich *et al*., 2012). Atwater and Heron (2011) showed that a simple thresholding of SNR3 is a good starting point, although a 20 dB limit constitutes a too severe QC criterion with a resulting detrimental impact on coverage area. Values of SNR3 below 10 dB have been proved to be closely linked to a significant decrease of the Multiple Signal Characterization (MUSIC) direction-finding algorithm skill (De Paolo and Terril, 2007). As MUSIC is employed to resolve ocean surface current structure (Schmidt, 1986), limitations in its performance are related to potentially suspect velocity outputs. Furthermore, different combinations of dynamic thresholds cutoffs have been analyzed to quantify the potential for error reduction (De Paolo *et al*., 2015). Since the question still remains open, further researches are currently underway to shed light on it.

In addition, the credibility of HF radar data has been previously tested in extensive validation studies, including direct comparisons of HF radar-derived surface currents with moored ADCP's, point-wise current meters – PCM hereinafter- or drifters (Graber *et al.*, 1997; Kaplan *et al.*, 2005; Cosoli *et al.*, 2010). Accordingly, a number of validation works with *in situ* current sensors have been performed with the HF coastal radar network operated by Puertos del Estado (Fig. 1 – a) -PdE hereinafter- in order to quantify and lower uncertainties in radar estimations at both the radial and total vector level (Alfonso *et al.*, 2006; Lorente *et al.*, 2014, 2015a and 2015b).

Correlation coefficients (CORR) and root mean squared errors (RMSE) have been previously found to be in the ranges [0.32-0.92] and [6-30 $cm \cdot s^{-1}$], respectively (Kohut and Glenn 2003; Paduan *et al.*, 2006; Chapman and Graber, 1997). Relative HF radar velocity errors can vary dramatically with the radar transmission frequency, sensor type and location within the sampled domain, as well as the data processing scheme used (Rypina *et al.*, 2014; Kirincich *et al.*, 2012). In this frame, the instrumental noise and sub-grid scale current variability have been reported to yield noise levels of 4-6 $cm \cdot s^{-1}$ (Emery *et al.*, 2004; Ohlmann *et al.*, 2007; De Paolo *et al.*, 2015).

~~The main goal of this work is to present a combined QC methodology for the specific case of Ebro HF radar (although easily expandable to the rest of PdE radar systems):~~

The main goal of this work is to explore basic features of the sea surface circulation in Ebro River estuary as derived from reliable and accurate HF radar surface current measurements. To this aim, a combined QC methodology is firstly applied: one year-long (2014) real-time web monitoring of nonvelocity-based diagnostic parameters and ~~regular~~ offline validation of HF radar-derived current data with *in situ* observations from a ~~point-wise current meter~~PCM, installed in a buoy moored within the radar domain (B1, Fig. 1 - b). This integrated approach is applied during 2014 in order to infer both radar site status and HF radar system overall performance and also to provide upper bounds on both radial and total radar current measurement accuracy (Lorente *et al.*, 2015c). Once HF radar data quality is estimated, Ebro Delta HF radar capabilities in reproducing well-known circulation features are investigated through the exploration of monthly averaged flow patterns and dominant modes of variability both in time and space (Cosoli *et al.*, 2012a and 2013; Kovacevik *et al.*, 2004). Lastly, the relative contribution of local wind as forcing mechanism is evaluated.

This paper is organized as follows: sections 2 and 3 outline the specific instrumentation and methods used in this study, respectively, followed in section 4 by a detailed discussion of the results. Finally, main conclusions are summarized in section 5.

2. Instrumentation.

2.1. HF radar.

A CODAR SeaSonde standard-range HF radar system was deployed at Ebro Delta in December 2013 within the frame of RIADE (Redes de Indicadores Ambientales del Delta del Ebro) project. The HF radar network consists of an array of three remote shore-based sites: Salou, Vinaroz and Alfacada. They will hereafter be referred to by their four letter site codes: SALO, VINA and ALFA, respectively (Fig. 1 - b).

Con formato: Normal, Espacio Antes: 10 pto, No ajustar espacio entre texto latino y asiático, No ajustar espacio entre texto asiático y números

Con formato: Fuente: (Predeterminado) Times New Roman, 12 pto

The HF radar technology, founded on principle of Bragg scattering of the electromagnetic radiation over a rough sea (Crombie, 1955), infer the radial current component from the Doppler-shift of radio waves back-scattered by surface gravity waves of half their electromagnetic wavelength. Each single radar site is configured to estimate radial currents moving toward or away from the receive antenna. Since the speed of the wave is easily derived from linear wave theory, the velocity of the underlying ocean surface currents can be computed by subtraction. The distance to the backscattered signal is determined by range-gating the returns and the angle of origin is inferred, in the case of CODAR SeaSonde radars, by a direction-finding process (Barrick and Lipa, 1997) using three collocated receive antennas (two orthogonal crossed loops and a single monopole) and the MUSIC algorithm (Schmidt, 1986).

Each site is operating at a nominal frequency of 13.5 MHz with a 90 KHz bandwidth, providing hourly radial measurements with a cut-off filter of 100 $cm \cdot s^{-1}$ and representative of current velocities in the upper first meter of the water column. Only calibrated (measured) antenna beam patterns (hereinafter APM) were employed by the manufacturer supplied software to process radial data used in the present study, with the aim of maximizing HF radar usefulness for operational applications (Lipa *et al.*, 2006; Kohut and Glenn, 2003). In regions of overlapping coverage from two or more sites, radial current measurements are geometrically combined using a least-square fit technique (Barrick and Lipa, 1986) with the averaging radius set to 6 km in order to estimate hourly averaged total current vectors on a predefined Cartesian regular grid with 3 x 3 km horizontal resolution. The maximum horizontal range is set to 80 km and the angular resolution is 5º.

HF radar-derived data used in this study have been collected from 1 January to 31 December 2014. During this period the three sites were simultaneously operational and radar coverage was as its maximum extent. Temporal data coverage was quantified by computing the percent of total possible vector returns at each radar grid point (Fig. 1 - b). Percent coverage decreases rapidly near the outer edges of the domain where error levels are higher due to poor intersecting beam geometry (Chapman and Graber, 1997) and quantified by larger Geometric Dilution of Precision (GDOP, Chapman *et al*, 1997). GDOP is an unit-less coefficient of uncertainty that characterizes how radar geometry may impact on measurements accuracy and position determination errors, owing to the angle at which the radials intersect and also to uncertainties in the radial vectors geometrically combined (Levanon, 2000; Trujillo *et al.*, 2004).

With the aim of screening out radar grid points where data are less reliable, a threshold on percent coverage has been imposed. Only time series of zonal and meridional surface currents at grid points with percent coverage greater than 50% over the 2014 annual record have been considered in this study. The selected coverage area present associated GDOP values of 1.5 or less.

2.2. Buoy B1.

The domain of Ebro Delta HF radar array includes an ocean Seawatch buoy deployed since August 2004 in the eastern waters of the Iberian Peninsula: Tarragona buoy (40.68ºN, 1.47ºE, 688 meters depth), hereafter referred to as B1 (Fig. 1 - b). This buoy is equipped with an acoustic point-wise current meter manufactured by Falmouth Scientific Inc., providing quality-controlled hourly averaged current velocity vectors at a nominal depth of three meters. A wind speed and direction sensor manufactured by R. M. Young Company measures hourly wind data at a nominal height of 3 meters. It should be noted that current and wind records from B1 are only available from 1 May to 31 October, 2014 (Fig. 1 - c).. B1 suffered from brief communication outages during this period and subsequent short gaps (2-3 h) in data time series have been linearly interpolated.

3. Methods.

3.1. Online Quality Control of HF radar measurements.

In order to ensure the reliability of the HF radar products delivered, maintenance and Quality Control (QC) procedures must be performed at various stages on the data generation pipeline. The manufacturer software package integrates a set of QC routines and thresholding techniques in the data processing chain (*e.g.*, limits for maximum vector magnitude and maximum GDOP).

This section presents a simplistic approach based on additional data quality checks at the post-processing stage and devoted to examine a variety of nonvelocity-based indicators provided by the manufacturer (CODAR Ocean Sensors -COS-) and listed in (Table 1). Such indicators include hardware, antenna, radial and total parameters, employed here as diagnostic tools for evaluating HF radar integrity and health (Roarty *et al*., 2012, Emery and Washburn, 2007). A dedicated online website has been developed to operationally monitor radar site status since anomalous values, inconsistencies or sharp fluctuations in the indicators might be related to potential malfunctions. This automated quality control web tool runs in background with a cron job, being updated on an hourly basis.

One year-long (2014) real-time monitoring has been performed in order to inspect the temporal evolution and consistency of the aforementioned parameters, obtain estimates of their standard ranges and evaluate Ebro Delta radar site performance according to them (Lorente *et al*., 2015a). Abrupt or gradual degradation and failure problems can be easily detected, triggering alerts for troubleshooting when defined thresholds (initially set to two standard deviations above/below the mean) are persistently exceeded. Particular emphasis has been devoted to SNR3 and the number of radial vectors provided.as it has been previously analyzed as valid proxy for radar data quality (Cosoli *et al*., 2012b).

Finally, automated quality checks have been implemented at the second level within the hierarchy defined for QC procedures, referred to total vectors. Temporal and spatial coverage of Ebro Delta radar system are separately analyzed on a monthly basis and later confronted to each other to check if HF radar systems operate within tolerance ranges, fulfilling the recommended level of data provision: 80% of the spatial region over the 80% of the time (Roarty *et al*., 2012).

3.2. HF radar validation.

HF radar measurements are subject to many potential errors as a consequence of inherent problems of radar technology, such as power-line disturbances, sea clutter, ship and ionosphere echoes or weather-depended and interference-sensitive coverage (Graber *et* *al*., 1997). Direct comparisons against other *in situ* sensors (ADCP's, point-wise current meters – PCM hereinafter , drifters or similar) permit an independent assessment of HF radar performance together with a quantitative estimation of uncertainties in radar current measurements.

Since the Ebro Delta HF radar footprint overlooks of a moored PCM within its spatial coverage, an accuracy assessment of radar surface currents is performed for a 6-month period May-October 2014 of concurrent radar-PCM measurements. The present section builds on previous investigations devoted to the determination of measurements errors, the evaluation of direction-finding capabilities and the angular distribution of radial velocity uncertainties (Emery *et al.*, 2004; Paduan *et al.*, 2006; Cosoli *et al.*, 2010; De Paolo and Terrill, 2007).

To this aim, the radar radial arc geographically closest to B1 buoy location has been selected for each HF radar site and radial current vectors estimated at each arc point have been compared with the radial projection of PCM velocities. The B1-HF radar comparative analysis allows the computation of statistical parameters (*e.g.*, CORR and RMSE) as a function of the angle comprised between B1 and the arc grid point position. In absence of direction-finding errors (DF), maximum CORR and minimum RMSE values should be found over the arc point closest to B1 location. In presence of DF, the bearing offset is thus expressed as the angular difference between the arc point with maximum correlation and the buoy location.

Radial current time series have been filtered to remove all tidal, diurnal and inertial fluctuations (the inertial period is 18.4 h at B1 location latitude) from the velocity data. Filtered time series, obtained after applying a 10^{th} order digital low-pass Butterworth filter with a cut-off period of 30 h (Emery and Thomson, 2001), have been compared to evaluate the discrepancies in subinertial currents.

Complementarily, HF radar total vector hourly estimations at the grid point closest to B1 location (HFR1, 1.48ºE 40.69ºN, Fig. 1 - b) have been compared with PCM velocities to provide upper bounds on the radar current measurement accuracy. Comparisons have been undertaken using zonal (U) and meridional (V) components in order to evaluate the agreement between both instruments by means of the computation of a set of statistical metrics – RMSE, scalar and complex correlations and best linear fit of scatter plots. Monthly results have been summarized with Taylor diagrams (Taylor, 2001), which provide a concise statistical summary of the agreement between both datasets.

Finally, rotatory spectral analyses (Gonella, 1972) have been performed for HF radar-derived total vectors at HFR1 location and for current data from B1 in order to identify the dominant modes of temporal variability. To ensure the continuity of the data record, small gaps detected (not larger than 6 h) in time series have been linearly interpolated. Spectra have been calculated by dividing time series into successive six day segments, with a 50% overlap and a Hanning window (Emery and Thompson, 2001), and subsequently averaged to provide some smoothing. Confidence levels for spectra densities have been derived assuming a chi-squared distribution for the variance.

3.3. Characterization of the surface circulation field

The ability of HF radar to reproduce well-known circulation features in Ebro Delta area has been investigated through the exploration of mean flow patterns and dominant modes of surface current variability. To this purpose, mMaps of the Eulerian mean current field have been constructed at monthly time scale from the raw radar time series on a subsampled grid with the aim of assessing the surface current dynamics in Ebro Delta. As previously mentioned, only radar grid points satisfying a minimum data return of 50% over the monthly record have been considered. Due to this constraint, the study area was not uniformly covered.

Additionally, a complex Empirical Orthogonal Function (EOF) decomposition (Kundu and Allen, 1976) has been used to infer the driving forces and spatiotemporal scales behind the variability of sea surface currents (Kaihatu *et al.*, 1998). This method, which reduces the components of the vector field to a complex scalar, has become widespread in order to extract the dominant modes of variability. The representative spatial patterns (or EOF modes) and their corresponding temporal coefficients (which describe the evolution of the modes) are determined by using the singular value decomposition of the covariance matrix. Each statistically significant EOF mode explains a limited portion of the total surface current variance.

EOF analysis has been applied to radar current velocity dataset using again the raw, (unfiltered) hourly time series for the entire year 2014. Main spatial modes obtained for HF radar have been interpreted in terms of physical processes related to the detected spatially coherent structures. Since the modes are uncorrelated, observed current fields can be reproduced by using the first few modes which contain a significant portion of the total variance. Since EOFs are purely statistical, each EOF mode's statistical significance must be evaluated. Several rules of thumb have been previously proposed indicating when an EOF is likely to be subject to large sampling fluctuations. In the present work, error estimates based on temporal decorrelation scales have been calculated according to North et al. (1982):

$$\delta(\lambda_i) = \lambda_i * (2/N)^{\frac{1}{2}} \qquad [1]$$

Where δ_i is the eigenvalue for mode i, and N is the number of degrees of freedom determined using a conservative two-day decorrelation time-scale, following Münchow and Chant (2000). If the confidence intervals from the error estimates of any modes overlap, the modes may be non-orthogonal and can not be considered distinct and uncorrelated. Consequently, such modes are excluded from the EOF analysis and hence only the first previous modes can be considered to contain a significant portion of the total variance and to properly reproduce the observed surface current fields.

Finally, hourly wind vector dataset registered at B1 buoy has been also decomposed into principal components in order to infer the main axis of variability. Particular emphasis has been placed on the relationship between wind and radar-derived current EOF modes of variability in order to derive a better statistical insight.

4. Results and discussion

4.1. Annual Quality Control

This analysis aims quantifying the consistency of nonvelocity-based diagnostic parameters over the nearly continuous 1-year time series, as indicators of HF radar regular status in terms of robustness and stable performance.

Since SNR3 has been previously analyzed as valid proxy for radar data quality (Cosoli *et al.*, 2012b), its evolution has been routinely monitored during 2014. Box plots of SNR3 for each radar site (Fig. 2 – a, b, c) exhibit a consistent monthly evolution, with a median (central mark) above 40 dB. However, a number of sharp decreases can be occasionally observed in VINA site for the month of June (Fig. 2 - c), exceeding the previously reported threshold of 10 dB (De Paolo and Terril, 2007).

The annual time serie of hourly SNR3 values for VINA site (Fig. 2 - d) reveals that the thresholds proposed in the present work (two standard deviations above/below the mean, represented by bold blue dotted lines) were abruptly exceeded several times in June. SNR3 reached extremely low values, leading to a drastic reduction in the radar spatial coverage presumably related to limitations in the MUSIC algorithm namely, the extraction of a maximum of two bearing solutions for a given range cell and a given radial current velocity. In this context, poor SNR3 values associated with potential interferences or environmental noise can lead to ambiguities in the estimation of the direction of arrival (DOA) function performed by MUSIC algorithm. Such ambiguities, based on the existence of more than two bearing solutions, eventually produce gaps in HF radar spatial coverage since additional solutions are excluded.

. Consequently, the number of radial vectors (NRV) provided by VINA lowered significantly in June (Fig. 2 - e). Leaving aside the regular high frequency fluctuations due to the day/night cycle, NRV was several times below 500 and even equal to zero, indicating a poorer than expected performance of VINA site during this month. Nonetheless, it appears to be a sporadic episode, maybe related to radio-wave interferences, since VINA presented a stable performance during the second semester of 2014.

The quality checks implemented at total vectors level allow an overall evaluation of Ebro Delta HF radar system performance on a monthly basis (Fig. 3). A comparative analysis for February and June confirms the degraded performance during the latter. Data availability generally exceeded 80% in time over the majority of the radar footprint in February, with an abrupt decrease at the periphery of the radar range (Fig. 3 - a). By contrast, it only outreached the 50% in June, with a smoother transition at the outer edges of the domain (Fig. 3 – b). The evolution of the spatial coverage was rather consistent in February, with sporadic decreases below 50% (Fig. 3 - c). On the contrary, an irregular performance is detected in June as a consequence of both ALFA site outage (1-8 June) and VINA irregular behavior (Fig. 3 - d). The first factor yielded a dramatic and persistent drop in the areal coverage, lower than 20% most of the time. The second led to a significant, albeit occasional, reduction in the radar spatial domain (below 50%), which can be observed from 8 to 30 June 2014.

Finally, the temporal and spatial coverage have been confronted to each other (Fig. 3 – e, f). Ebro Delta radar system was closer to fulfill the required 80%-80% level of data provision in February (Roarty *et al.*, 2012), with a 64% of the areal domain (referred to its maximum extent) available the 80% of the time. By contrast, the radar system barely reached the 35% of spatial coverage for the 80% of the time in June. Despite this occasional degradation, radar sites overall performance and their day-to-day operation have been found to be robust and within tolerance ranges, with sporadic interruptions (presumably attributable to power outages) that introduced short-duration gaps in time and space.

It is noteworthy that the described methodology, at this preliminary development stage, is not able to remove suspicious values (outliers, spikes or spurious values) from the data stream in real time like Cosoli *et al.* (2012b) but only to detect anomalies and categorize them in order to create a historic database of flagged radial files similar to ~~a historic radial database similar to~~ Roarty *et al.* (2012) for a later offline reprocessing of total vector maps when one (or more) radar site(s) is (are) considered to be working abnormally.

In this context, the hourly radial vectors provided by VINA site in June that did not satisfy the proposed QC control have been discarded from the analyses performed in the next sections and the associated total vector maps have been accordingly reprocessed offline. Future efforts should be devoted to improve radial data quality in real-time prior to the vector combination process and also to assign meaningful quality descriptor flags for each grid point data in total current fields.

4.2. Buoy-radar comparison results

~~In order to assess the reliability of radar surface currents, an error analysis is first performed on the radial velocities from individual radar sites for the 6-month radar-buoy common period (Cosoli *et al.*, 2012a).~~ The evaluation of direction-finding capabilities revealed the existence of small bearing errors (hereafter $\Delta\alpha$) in radar radial estimations, ranging between 2°-8° (Fig. 4) and in accordance with the typical values previously reported (Emery et al., 2004; Paduan *et al*., 2006).

Comparison of unfiltered hourly radial currents estimated by B1 and SALO site (Fig. 4 - b) shows maximum CORR in a grid point (denoted by vertical solid red line) angularly close to B1 location (vertical dotted black line): 0.79, with associated RMSE of 10.95 $cm \cdot s^{-1}$ and $\Delta\alpha$ of 3.74º in the counter-clockwise direction. VINA site (Fig. 4 - c) presents a lower bearing offset ($\Delta\alpha$ = 1.82º) but also lower (higher) CORR (RMSE) value of 0.58 (13.31 $cm \cdot s^{-1}$). It is worth mentioning that minimum RMSE values are also placed on the vicinity of the correlation peaks. The VINA site exhibits the largest pointing error ($\Delta\alpha$ = 7.82º) and the poorest agreement with moored radial estimations as CORR is 0.58 and RMSE is fairly above 18 $cm \cdot s^{-1}$ (Fig. 4 - d).

Hourly time series of low-pass filtered radial currents measured by B1 and those estimated in the closest range arc point ("best match-angle") by each HF radar site are presented in Fig. 5. Metrics derived from the accuracy assessment highlight the consistently high agreement between SALO radar site and B1 estimations, with a CORR and RMSE values of 0.80 and 5.58 $cm \cdot s^{-1}$, respectively (Fig. 5 - a). Results derived from the best linear fit reveal a slope close to 1 and an intercept up to -0.82 $cm \cdot s^{-1}$. The concordance between ALFA site and B1 is moderately good, with acceptable pairs of values CORR-RMSE and slope-intercept: [0.63-6.91] $cm \cdot s^{-1}$ and [0.73-1.92] $cm \cdot s^{-1}$, respectively (Fig. 5 - b). VINA site data show lower agreement with *in situ* measurements (Fig. 5 - c) as reflected by a lower (higher) CORR (RMSE) value of 0.56 (7.76 $cm{\cdot}s^{-1}$). This might be partially attributable to the long site-buoy distance (*i.e.*, the radar signal is weaker) and to the limited radar data availability due to day/night coverage fluctuations (*i.e.*, the data return is more than three times lower, with only 986 hourly observations available).

Ancillary validation works with radial measurements like internal self-consistency checks have not been performed due to Ebro Delta radar sites' geometry. Radar-to-radar comparisons along the overwater baselines (Paduan *et al*., 2006; Yoshikawa *et al*., 2006; Atwater and Heron, 2010), although valuable to explore quantitatively intrinsic uncertainties in radial velocities, are not feasible since they are positioned over land or near the coastline.

Statistical metrics derived from filtered hourly time series comparison of zonal (U) and meridional (V) components of total vectors estimated by B1 and HFR1 for the 6-month period are presented in Fig. 6. Results reveal a good agreement for both components (CORR above 0.74), in accordance with results reported in the literature (Cosoli *et al*., 2010; Kaplan *et al*., 2005). RMSE is significantly higher for the zonal component than the meridional: 12.69 versus 4.02 $cm{\cdot}s^{-1}$ (Fig. 6 – a, b). The disparity of uncertainty levels between the east and north component vectors comes for the geometry of the radar vector combination and the prevalent south-southwestward current flow. This presumably might lead to less (more) precise radial vectors provided by ALFA (SALO) radar site since radial measurements are proved to be more accurate when the dominant current flow moves in the same direction (Robinson *et al*., 2011). Since ALFA (SALO) site contributed mainly to the HF radar zonal (meridional) current assessment in B1 nearby region, a strong relationship between radial and total vector uncertainties has been evidenced.

The scatter plots (not shown) and the associated best linear fits show that HF radar slightly underestimates total current velocities registered by B1 since the slopes are below 1: 0.71 and 0.67 for U and V components, respectively. The time-averaged complex correlation coefficient between B1 and HFR1 currents at zero lag is 0.77. The related phase is 8.65º, indicating that the former are, on average, slightly right shifted since the veering angle gives the average counter-clockwise turning of the second vector with respect to the first vector (Kundu, 1976).

The monthly mean current values were computed to characterize the main features of the flow in this region. The descriptive statistics reveal predominant negative values for the zonal speed (Fig. 6 - c) and a quasi-permanent average flow in the N-S direction (Fig. 6 - d). There is no evidence of a seasonal signal in both zonal and meridional velocity components of radar and B1 surface currents. Therefore, both instruments exhibit similar monthly mean values and variability, capturing the well-known southwestward thermohaline flow and identifying episodic but intense current reversals, as those observed by mid-September (Fig. 6 – a, b).

The monthly comparison of total vectors, performed on the unfiltered time series, provide a variety of metrics that are concisely summarized in a Taylor diagram (Taylor, 2001), shown in Fig. 7. The diagram compares both data sets by combining information about their relative standard deviations, centered RMSE and CORR, synthetizing the statistical information of how closely the radar measurements at HFR1 grid point match with B1 velocities. As it can be seen, the cluster of points that show best agreement (*i.e.*, are closest to their corresponding reference point, labeled with blue squares) are those corresponding to the period May-September (red squares, sequentially numbered 1-5). The reported correlation coefficient, standard deviation and RMSE values emerge in the ranges of [0.72-0.83], [10.96-14.18 cm·s^{-1}] and [7.48-8.75 cm·s^{-1}], respectively, for both zonal and meridional velocity components (Fig. 7 – a, b). However, HF radar is less accurate by the last month of the analyzed period, since metrics computed for October (red square 6) reflect lower (higher) CORR (RMSE) values: 0.50-0.58 (10.92-11.03).

Instrument-to-instrument comparisons present intrinsic limitations since both devices operate differently and at distinct nominal depths. A fraction of observed radar-B1 differences can thus be explained in terms of different sampling strategies on disparate time and space scales (Ohlmann *et al.*, 2007). In this context, many of the uncertainties associated with HF radar technology are geometric in nature. Apart from the instrumental noise, other sources of potential errors in vector currents might be the sub-grid horizontal shear, the geophysical variability within the water column (Graber *et al*, 1997) and some specific processes, namely, the Stokes drift, the Ekman drift and baroclinity (Paduan *et al.*, 2006).

Spectral analyses have been computed for a 6-month period May-October 2014 (warm stratified season) to examine power spectral discrepancies in the frequency domain between both instruments. B1 and HFR1 current time series present qualitatively similar characteristics, capturing properly the dominant features within the diurnal and inertial bands, related to significantly prevalent clockwise (CW) rotatory motions (solid lines, Fig. 8). Relevant polarized peaks are evident for both datasets, although their amplitudes are slightly larger for radar currents (solid red line). The inertial peak is the most pronounced, pointing out the adjustment of the stratified fluid to the wind driven currents and, subsequently, the importance of local wind as forcing mechanism (addressed in section 4.3.2). Offshore oscillations in this frequency band are a common feature in ocean circulation and their presence in the study area has been previously documented (Font *et al.*, 1990). By contrast, the counter-clockwise component (CCW, dotted lines) is much less energetic (especially in the case of B1 current estimations) and is where the main radar-B1 differences in variance distribution can be found. Finally, a drop of energy and later flattening about 2 cpd are common for the CW components of both B1 and radar spectra although the latter presents larger energy at that frequency band. Radar surface estimations are influenced by energetic high-frequency processes related to air-sea interaction like highly variable and strong wind gusts, which are not fully contained in sub-surface current estimations provided by the current meter..

4.3. Dominant features of the surface flow

4.3.1. Monthly averaged current patterns

The sequence of monthly averaged current maps in Fig. 9 shows that some of the main circulation features in Ebro Delta remain rather invariant throughout most part of the year, like the southwestward slope jet, associated with the highest velocities detected (above 30 cm·s^{-1}). The current speed diminishes toward coastal areas, except in the vicinity of ALFA radar site, where the signal of Ebro River impulsive-type freshwater outflow is clearly evidenced during winter and spring (Fig. 9 - a, b, f). As a consequence of the remarkable seasonal variability of Ebro discharge rates, the estuarine plume loses intensity during the warm season (Fig. 9 - c), becoming barely noticeable in late summer and early autumn (Fig. 9 – d, e), until the beginning of the following hydrological cycle (Fig. 9 - f).

It is noteworthy the weakening of the southwestward slope jet during the central part of the year, in agreement with reported short periods of current reversals (Font *et al.*, 1990). The jet is intensified in October, perhaps –as a result of the observed increase of the mesoscale activity (Font *et al*., 1995), reaching ultimately a peak strength in December. By the end of 2014, the monthly spatial patterns become rather uniform, revealing the acceleration of the jet (with a spatial propagation of maximum velocities, exceeding 40 cm·s^{-1}) on the eastern region of the radar domain and also the presence of two small-scale coastal meanders (Fig. 9 - e, f).

A coastal anticyclonic eddy can also be observed in radar data, confined south of Ebro Delta mouth (Fig. 9 – a, b, c). This hydrodynamic feature has been well-documented in previous studies (Font et al., 1990; Salat et al., 2002), which stated the interaction of the buoyancy-driven flow with the topography as triggering source of this clockwise gyre, This well-documented hydrodynamic feature is due to the interaction of the buoyancy-driven flow with the topography, reinforcing the shelf/slope front that drives the general circulation to the south-southwest (Font *et al.*, 1990; Salat *et al*., 2002). In addition, persistent and high-intensity NW wind jets, dominant during the October-May cold season and channeled by the narrow Ebro Valley, have been reported to introduce negative vorticity in the flow south of the Ebro Delta and reinforce the long-time preservation of this small-scale eddy (Garcia and Ballester, 1984; Espino *et al*., 1998). Notwithstanding, this coastal clockwise rotation is eventually absent from September (not shown) to December monthly averaged current maps.

During the transition month of August, a large anticyclonic recirculation cell is evidenced, detached from the shore and located on the center of radar domain (Fig. 9 - d). This current pattern is dominated by the interaction of the cross-shelf flow on the southern inner shelf with topographic obstacles, giving rise to a shift to the right of the coastal flow. The subsequent northeastward reversal of the inshore flow is scarcely influenced by Ebro River freshwater discharge as it reaches the lowest value at this stage of the year.

4.3.2. Empirical orthogonal function (EOF) analysis

The mean and EOFs of hourly surface currents have been calculated for a 1-year time period (2014) when the three radar sites were simultaneously operational (Fig. 10). The long-term mean flow (Fig. 10 - a) captures the main circulation features previously reported about 'the North Current', characterized by a quasi-permanent shelf-slope jet oriented southwestward and a remarkable Ebro River impulsive-type freshwater discharge (located in front of ALFA site). The buoyancy input introduced by large estuarine outflows, together with topographic effects, lead to the development of the aforementioned anticyclonic coastal eddy on the southern side of the delta.

Since the EOF analysis has been performed on the unfiltered data set containing significant high-frequency spatiotemporal variability, the first three EOFs cumulatively account only for the 46.1% of the total variance (26.1%, 15.3% and 4.7%, respectively). H Only the first three EOF modes are statistically significant according to the mode selection rule and truncation criterion suggested by North et al. (1982). The first, second and third modes are distinct and uncorrelated; however, the fourth mode is not since its error bars overlap with those of mode 5 (not shown). Therefore, higher order modes will not be further addressed here as they represent a combination of unresolved high-frequency motions or noise (Cosoli *et al.*, 2012a).

The first dominant EOF mode (Fig. 10 - b) represents a spatially uniform pattern, rather similar to the annual averaged current map, with an alongshore shelf-slope jet flowing mainly southwestward, basically capturing the thermohaline Catalan front. The second EOF (Fig. 10 - c) shows a homogeneous spatial structure, perpendicular to the first mode, with a well-defined offshore-directed flow~~ presumably driven by persistent and intense (up to 100 km/h) northwesterly winds (called 'mistral winds') channeled by the narrow Ebro Valley (Font, 1990)~~. The spatial pattern of EOF3 (Fig. 10 - d) adds some complexity to the basic uniform flows represented by the first two modes, since it introduces curvature to the current field by means of a large, albeit weak, anticyclonic recirculation cell (flow divergence) in the central (southern) region of the radar domain.

Temporal variation in the strength of these three EOF modes is represented by their corresponding principal components~~time coefficients~~, shown in Fig. 11. EOF1 is predominantly positive except during the summertime, when the quasi-permanent flow to the SW is altered by clockwise inertial oscillations (positive EOF3) and some periods of current reversals, with maximum occurrence during the stratified warm season as reported by ~~(~~Font *et al.*~~,~~ (1990). Nevertheless, EOF1 becomes again strongly positive during the autumn, reaching a peak by mid-December, in clear agreement with the strengthened shelf-slope jet flowing southwestwards shown in Fig. 9 - f. The temporal structure of EOF2 reveals a principal offshore-directed flow through January-May period and also in late December, coincident with the cold season (October-May) which is characterized by both energetic Mistral winds and Ebro River high discharge rates~~as response to both mistral energetic wind, dominant during the cold season (October-May), and Ebro River high discharge rates~~. Lastly, EOF3 adds clockwise curvature most part of the year (February-September and November). The evident enhancement of the anticyclonic gyre in August (positive EOF3), combined with the onshore-directed flow (negative EOF2) and the reversal of the main current flow (negative EOF1) during that time period, gave rise to a complex circulation scheme, rather similar to the monthly averaged pattern represented in Fig. 9 - d.

In order to define the prevalent wind directions registered at B1, the major and minor variance axes have been determined (Fig. 12 - a). The results show that the main variability occurs along a direction 99º azimuth containing the 54% of the total energy. This is the EOF1 mode, largely aligned with persistent and intense northwesterly mistral winds channeled by the narrow Ebro Valley (Font, 1990). The orthogonal EOF2 mode is oriented 9º clockwise from north and holds the remaining 46% of the variance, capturing mainly the influence of alongshore winds.

Linear correlation coefficients have been computed between the principal components related to the two main wind EOF modes of variability and radar-derived EOF2, since the cross-shelf circulation shown in Fig. 10-c might be presumably driven by strong local winds. The high correlation between the filtered principal components can be readily seen in Fig. 12 (b-c), with a value of 0.47 (0.67) for wind-PC1 (PC2) and radar-PC2, respectively. The results underline that the surface current variability in Ebro Delta can be influenced by wind action, in accordance with Espino et al. (1998), who demonstrated such relationship when winds are strong and steady enough. The higher agreement between both wind-radar PC2 appears to be consistent with Ekman transport to the right of the wind direction. By contrast, northwesterly mistral wind events (PC1) are expected to enforce the prevalent offshore-directed circulation regime (radar EOF2) by increasing the mean speed of the flow.

Equally, the influence of local wind forcing on HF radar EOF1 mode has been assessed (but not shown), with a correlation coefficient of 0.52 (-0.28) for wind PC1 (PC2). This finding highlights the impact of mistral winds on the predominant southwestward flow, by inducing an Ekman veering.

5. Summary and concluding remarks

Since ~~radar measurements are prone to errors,~~ the acquisition of high-quality surface current data remains as a priority for HF radar operators and the research community,~~.~~ ~~In the present work,~~ a combined quality control (QC) methodology has been ~~presented~~ applied for a three site standard-range (13.5 MHz) CODAR SeaSonde HF radar network deployed at Ebro Delta (NE Spain). This integrated approach consists of one year-long (2014) real-time web monitoring of nonvelocity-based diagnostic parameters, coordinated with a a 6-month (May-October 2014) ~~regular~~ offline validation of HF radar data (at both the radial and total vector levels) with independent *in situ* observations from a point-wise current meter installed in B1 buoy, moored within the radar footprint.~~.~~

Con formato: Párrafo de lista, Ajustar espacio entre texto latino y asiático, Ajustar espacio entre texto asiático y números

The overall stable and accurate performance of Ebro Delta HF radar during 2014, derived from the combined QC-validation approach, suggests that sites were functioning properly and that their APMs were correctly performed and integrated in the data processing. This provides ground truth to examine future radar performances.

Con formato: Fuente: (Predeterminado) Times New Roman, 12 pto

~~Signal-to-noise ratio at the monopole (SNR3) has been routinely monitored as it has been proved to be a valid indicator of both radar site status and HF radar system overall performance. Box plots of SNR3 for each radar site exhibited a consistent monthly evolution for 2014, although a number of sharp decreases have been occasionally detected in June for VINA site, exceeding the previously reported threshold of 10 dB and the limits of two standard deviations proposed in the present work. The abrupt drop in SNR3 values of VINA impacted negatively on the number of radials provided and, subsequently, in the spatiotemporal coverage of total current vectors during June. Notwithstanding, it seems to be a sporadic episode since the overall performance of radar sites and their day-to-day operation have been found to be robust and within tolerance ranges. One year of continuous operation revealed three sites up and operational in excess of 95% of the time, with occasional interruptions that introduced short-duration gaps in time and space.~~

~~Complementarily, a regular offline validation of HF radar-derived current data with independent *in situ* instruments is essential in order to provide lower bounds on radar current measurement uncertainties. To this aim, an accuracy assessment of Ebro Delta radar system estimations was attempted by means of comparison with measurements from a point-wise current meter installed in B1 buoy, moored within the radar footprint, for a 6-month period May-October 2014 when they were operating simultaneously.~~

The comparison was carried out at both the radial and total vector levels. Regarding the former, the directional accuracy of the HF radar was rated at better than 8º, suggesting that radar sites were functioning properly and that their APMs were correctly performed and integrated in the data processing. The correlation coefficient and RMSE values emerged in the ranges [0.58-0.79] and [10.95-18.31] cm·s^{-1}, respectively. Concerning the total velocity vectors, hourly current time series were compared for a single grid point in the HF radar domain corresponding to B1 location. The zonal and meridional components of radar surface currents tracked B1 subsurface currents fairly well. The correlation coefficient and RMSE values lied in the ranges [0.72-0.83] and [4.02-12.69], respectively, consistent with previously reported values (Kaplan *et al*., 2005; Cosoli *et al*., 2010), indicating that both instruments were indeed producing valid measurements of the current field during the concurrent period of records. Both systems described a predominant southwestward flow, with similar monthly mean values and variability. Therefore, Ebro Delta HF radar proved to have very satisfactory level of accuracy. The overall stable and accurate performance for 2014, derived from the combined QC-validation approach, provides ground truth to examine future radar performances.

The analysis of the monthly averaged spatial patterns of the velocity field shows that the HF radar properly represents basic oceanographic features and recurrent circulation patterns previously observed in the study area, namely: the predominant southwestward flow, the coastal clockwise eddy confined south of Ebro Delta mouth or the Ebro River impulsive-type freshwater discharge. It is also noteworthy that this study has been performed in a low-energy shelf where the surface currents are generally weaker than most of those referenced herein (Lorente *et al*., 2014). The EOF analysis related the flow response to local winds and confirmed that the surface current field evolved in space and time according to three dominant modes of variability, which significantly account for the 46.1% of the variance.

The EOF analysis confirmed that the surface current field evolved in space and time according to three dominant modes of variability, which account for the 46.1% of the variance. A year-round overall prevailing shelf-slope jet flowing southwestward is described by the first mode (21.6% of the variance), with the other two modes superimposed onto it, accounting for the 15.3% and 4.7% of the variance, respectively. The second mode captures the cross-shelf circulation induced by intense and persistent northwesterly winds while the third introduces complexity to the rather uniform pattern described by the first two modes by adding divergence and vorticity to the surface current field.

Regarding Ebro Delta study area, active and planned efforts are devoted to an extensive description of a variety of marine processes impacting on the evolution and reshape of the nearshore deltaic area: the wave action eroding exposed wetlands, the sediment transport, the freshwater discharges and buoyancy fluxes (which further complicate water motions in the Ebro Estuary) and ultimately the major influence of local wind forcing.

With respect to HF radar, it has been steadily gaining recognition as an efficient land-based remote sensing instrument for mapping surface currents at high spatial and temporal resolutions in near real time. This technology has become a core operational component of integrated multi-platform ocean observing systems thanks to its ability for long term coastal environmental monitoring of the spatially evolving surface current field, providing hence a dynamical framework for other observational networks (Shay *et al*., 2002).

Future works should include the use of verified HF radar data for the rigorous skill assessment of operational ocean circulation systems currently running in Ebro estuarine region like IBI (Iberia–Biscay–Ireland) regional system (Sotillo *et al*., 2015), implemented within the frame of MyOcean projects and the Copernicus Marine Environmental Monitoring Service (CMEMS). ~~Additional development efforts should address the rigorous skill assessment of operational ocean circulation systems currently running in Ebro estuarine region like MyOcean IBI (Sotillo *et al*., 2015).~~ A combined observational and modeling approach would provide a comprehensive characterization of the coastal circulation and benefit from the complementary nature of both systems. HF radar observations improve the model description by resolving low scale processes in areas with significant topographic gradients, whereas model outputs provide a 3-D qualitative picture with vertical resolution that completes the surface radar-derived information when the quality data or the spatiotemporal coverage are poorer.

This integrated strategy might complement and optimize the intense monitoring activity performed around the deltaic coastline through the timely and seamless delivery of high-quality operational products, devoted to support wise decision-making and mitigate anthropogenic hazards in the marine environment. Such products could also provide paramount information on biological connectivity between Ebro Delta marine protected area and other relevant ecological regions in the western Mediterranean Sea.

Acknowledgment

The authors gratefully acknowledge Qualitas Remos Company (partner of CODAR Ocean Sensors) for their useful suggestions and deeply appreciate comments provided during the paper revision process by Dr. Donald Barrick, Dr. Jeffrey Paduan and Dr. Guillaume Charria, which significantly improved the quality of the manuscript. The Spanish Ministerio de Economía y Competitividad supported this study through the OPErational RAdars for research in marine sciences (OPERA) project (CTM2012-33223).

References

Alfonso, M., Álvarez-Fanjul, E., and López, J.D.: Comparison of CODAR SeaSonde HF Radar operational waves and currents measurements with Puertos del Estado buoys, Final Internal Report of Puertos del Estado, 1-32, 2006.

Atwater, D.P., and Heron, M.L.: HF radar two-station baseline bisector comparisons of radial components, Proceedings of IEEE Oceans 2010, Sydney, Australia, pp 1-4, 2010.

Atwater, D.P., and Heron, M.L.: A first approach to SeaSonde quality control, Proceedings of IEEE Oceans 2011, Waikoloa, HI, USA, pp 1-5, 2011.

Barrick, D.E., and Lipa, B.J.: Correcting for distorted antenna patterns in CODAR ocean surface measurements, IEEE Journal of Oceanic Engineering, OE-11: 304–309, 1986.

Barrick, D., Fernandez, V., Ferrer, M.I., Whelan, C., and Breivik, Ø.: A short-term predictive system for surface currents from a rapidly deployed coastal HF radar network, Ocean Dynamics, vol. 62, no. 5, pp. 725–740, 2012.

Chapman, R.D. and Graber, H.C.: Validation of HF radar measurements, Oceanography, 10, N. 2: 76–79, 1997.

Chapman, R.D., Shay, L.K., Graber, H.C., Edson, J.B., Karachintsev, A., Trump, C.L., and Ross, D.B.: On the accuracy of HF radar surface current measurements: intercomparison with ship-based sensors, Journal of Geophysical Research 102 (C8), 18737–18748, 1997.

Codar Ocean Sensors: SeaSonde Diagnostic Files, CODAR Internal Document, May, 2005.

Cosoli, S., Mazzoldi, A., and Gacic, M.: Validation of surface current measurements in the Northern Adriatic Sea from High Frequency radars, Journal of Atmospheric and Oceanic Technology: 27–908, 2010.

Cosoli, S., Gacic, M., and Mazzoldi, A.: Surface current variability and wind influence in the north eastern Adriatic Sea as observed from high-frequency (HF) radar measurements, Continental Shelf Research, 33: 1–13, 2012a.

Cosoli, S., Bolzon, G., and Mazzoldi, A.: A Real-Time and Offline Quality Control Methodology for SeaSonde High-Frequency Radar Currents, Journal of Atmospheric and Oceanic Technology, 29, pp. 1313–1328, 2012b.

Cosoli, S., Licer, M., Vodopivec, M., and Malacic, V.: Surface circulation in the Gulf of Trieste (northern Adriatic Sea) from radar, model, and ADCP comparisons, Journal of Geophysical Research, Vol. 118, 11, pp. 6183-6200, 2013.

Crombie, D.D.: Doppler spectrum of sea echo at 13.56 Mc/s. Nature, 175, 681-682, 1955.

De Paolo, T., and Terrill, E.J.: Skill assessment of resolving ocean surface current structure using compact-antenna-style HF radar and the MUSIC direction-finding algorithm, Journal of Atmospheric and Oceanic Technology, 24: 1277–1300, 2007.

De Paolo, T., Terril, E., and Kirincich, A.: Improving SeaSonde radial velocity accuracy and variance using radial metrics, IEEE Oceans 2015, Genova, pp 1-9, 2015.

Emery, B., Washburn, M.L., and Harlan, J.A.: Evaluating radial current measurements from CODAR high frequency radars with moored current meters, Journal of Atmospheric and Oceanic Technology, Vol. 21: 1259–1271, 2004.

Emery, B.M., and Washburn, L.: Evaluation of SeaSonde Hardware Diagnostic Parameters as Performance Metrics, NOAA IOOS final report, October 2007.

Emery, W.J., and Thomson, R.E.: Data Analysis Methods in Physical Oceanography, Elsevier Science, Amsterdam, 2001.

Espino, M., Sanchez-Arcilla, A., and Garcia, M.A.: Wind induced mesoscale circulation off the Ebro Delta, NW Mediterranean: a numerical study, Journal of Marine Systems, 16, 235–251, 1998.

Font, J., Salat, J., and Tintore, J.: Permanent features of the circulation in the Catalan Sea, Pelagic Mediterranean Oceanography, Oceanologica Acta 9 (vol. sp.), 51-57, 1988 (a).

Font, J., Salat, J., and Wang, D.P.: Lagrangian and Eulerian observation of inertial oscillations in the shelf break offshore the Ebro River Delta (Catalan Sea, NW Mediterranean), Rapp. Comm. Int. Mer Médit 31: 201, 1988 (b).

Font, J.: A comparison of seasonal winds with currents on the continental slope of the Catalan sea (Northwestern Mediterranean), Journal of Geophysical Research, Vol 95, NO C2, pp. 1537-1545, 1990.

Font, J., Garcia-Ladona, E. and Gorriz, E.G.: The seasonality of mesoscale motion in the Northern Current of the Western Mediterranean: several years of evidence, Oceanologica Acta, Vol 18, N2, 207-219, 1995.

Garcia, M.A. and Ballester A.: Notas acerca de la meteorología y la circulación local en la región del Delta del Ebro, Invest. Pesquera (now Sci. Mar.) 48 (3), 469-493, 1984.

Gomez, R., Helzel, T., Petersen, L., Kniephoff, K., Merz, C.R., Liu, Y., and Weisberg, R.H.: Real-time quality control of current velocity data on individual grid cells in WERA HF radar, Oceans 2014, Taipei, pp. 1-7, 2014.

Gomez, R., Helzel, T., Merz, C.R., Liu, Y., Weisberg, R.H., and Thomas, N.: Improvements in ocean surface radar applications through real-time data quality-control, Conference: Current, Waves and Turbulence Measurement (CWTM), IEEE/OES, Florida, USA, March 2015.

Gonella, J.: A rotary-component method for analyzing meteorological and oceanographic vector time series, Deep Sea Research, Part II, 19: 833– 846, 1972.

Graber, H.C., Haus, B.K., Shay, L.K. and Chapman, R.D.: HF radar comparisons with moored estimates of current speed and direction: Expected differences and implications, Journal of Geophysical Research, 102, Nº C8, 18: 749–766, 1997.

Jimenez, J.A., Guillen, J., Sanchez-Arcilla, A., Gracia, V., and Palanques, A.: Influence of benthic boundary layer dynamics on wind-induced currents in the Ebro Delta inner shelf, Journal of Geophysical Research, Vol. 107, C6, 3054, 1-10, 2002.

Kaplan, D.M., Largier, J., and Botsford, L.W.: HF radar observations of surface circulation off Bodega Bay (northern California, USA), Journal of Geophysical Research, 110, C10020: 1-25, 2005.

Kaplan, D.M., and Lekien, F.: Spatial interpolation and filtering of surface current data based on open-boundary modal analysis, Journal of Geophysical Research: Oceans (1978–2012), vol. 112, no. C12, 2007.

Kaihatu, J.M., Handler, R.A., Marmorino, G.O., and Shay, L.K.: Empirical orthogonal function analysis of ocean surface currents using complex and real-vector methods, Journal of Atmospheric and Oceanic Technology, 15, 927–941, 1998.

Kirincich, A. R., de Paolo, T., and Terrill, E.: Improving HF Radar Estimates of Surface Currents Using Signal Quality Metrics, with Application to the MVCO High-Resolution Radar System, Journal of Atmospheric and Oceanic Technology, 29, 1377–1390, 2012.

Kohut, J.T., and Glenn, S.M.: Improving HF radar surface current measurements with measured antenna beam patterns, Journal of Atmospheric and Oceanic Technology, 20: 1303–1316, 2003.

Kovačević, V., Gačić, M., Mancero Mosquera I., Mazzoldi, A., and Marinetti, S.: HF radar observations in the northern Adriatic: surface current field in front of the Venetian Lagoon, Journal of Marine Systems, Volume 51, Issues 1–4, pp 95–122, 2004.

Kundu, P.: Ekman veering observed near the ocean bottom, Jounal of Physical Oceanography, 6, pp. 238-242, 1976.

Kundu, P.K., and Allen, J.S.: Some three-dimensional characteristics of low-frequency current fluctuations near the Oregon coast, Journal of Physical Oceanography 6, 181-199, 1976.

Levanon, N.: Lowest GDOP in 2-D scenarios. IEEE Proceedings, Radar, Sonar Navigation, 147(3): 149–155, 2000.

Lipa, B., Nyden, B., Ullman, D.S., and Terrill, E.: SeaSonde radial velocities: derivation and internal consistency, IEEE Journal of Oceanic Engeneering, 31 (4): 850–861, 2006.

Liu, Y., Weisberg, R.H., and Merz, C.R.: Assessment of CODAR SeaSonde and WERA HF Radars in Mapping Surface Currents on the West Florida Shelf, Journal of Atmospheric and Oceanic Technology, 31, 1363–1382, 2014.

Lorente, P., Piedracoba, S., Soto-Navarro, J., and Alvarez-Fanjul, E.: Accuracy assessment of high frequency radar current measurements in the Strait of Gibraltar, Journal of Operational Oceanography 7 (2), 59–73, 2014.

Lorente, P., Piedracoba, S., Soto-Navarro, J., Ruiz, M.I., Alvarez-Fanjul, E., and Montero, P.: Towards the implementation of a fully operational HF coastal radar network operated by Puertos del Estado, IEEE Oceans 2015, Genova, pp 1-6, 2015a.

Lorente, P., Piedracoba, S., Alvarez-Fanjul, E.: Validation of high-frequency radar ocean surface current observations in the NW of the Iberian Peninsula, Continental Shelf Research 92, pp. 1-15, 2015b.

Lorente, P., Piedracoba, S., Soto-Navarro, J., and Alvarez-Fanjul, E.: A combined QC methodology in Ebro Delta HF radar system: real time web monitoring of diagnostic parameters and offline validation of current data, European Geosciences Union General Assembly (EGU), Vienna, April 2015c.

Marmain, J., Molcard, A., Forget, P. and Barth, A.: Assimilation of HF radar surface currents to optimize forcing in the North Western Mediterranean sea, Nonlin. Processes Geophys., Vol. 21, pp. 659-675, 2014.

Münchow, A. and Chant, R.J.: Kinematics of inner shelf motions during the summer stratified season off New Jersey, J. Phys. Oceanogr., 30, pp. 247-268, 2000.

North, G.R., Bell, T.L., Cahalan R.F. and Moeng, F.J.: Sampling errors in the estimation of empirical orthogonal functions, Mon. Wea. Rev. 110, pp. 699-706, 1982.

Ohlmann, C., White, P., Washburn, L., Terril, E., Emery, B., and Otero, M.: Interpretation of coastal HF radar-derived currents with high-resolution drifter data, Journal of Atmospheric and Oceanic Technology, 24: 666-680, 2007.

Paduan, J.D., Kim, K.C., Cook, M.S., and Chavez, F.P.: Calibration and validation of direction-finding High-Frequency radar ocean surface current observations, IEEE Journal of Oceanic Engineering, 31, N. 4: 862–875, 2006.

Robinson, A.M., Wyatt, L.R., and Howarth, M.J.: A two year comparison between HF radar and ADCP current measurements in Liverpool Bay. Journal of Operational Oceanography, 4: 33–45, 2011.

Con formato: Normal, No ajustar espacio entre texto latino y asiático, No ajustar espacio entre texto asiático y números

~~Salat, J., Garcia, M.A., Cruzado, A., Palanques, A., Arín, L., Gomis, D., Guillen, J., de León, A., Puigdefàbregas, J., Sospedra, J., and Velásquez, Z.R.: Seasonal changes of water mass structure and shelf-slope exchanges at the Ebro Shelf (NW Mediterranean), Continental Shelf Research 22 (2002), 327-348, 2002.~~

Roarty, H., Smith, M., Kerfoot, J., Kohut, J., and Glenn, S.: Automated Quality Control of High Frequency Radar Data, IEEE Oceans 2012, pp. 1-7, 2012.

Rypina, I.I., Kirincich, A. R., Limeburner, R. and Udovydchenkov, I. A.: Eulerian and Lagrangian Correspondence of High-Frequency Radar and Surface Drifter Data: Effects of Radar Resolution and Flow Components, Journal of Atmospheric and Oceanic Technology, 31, 945–966, 2014.

Salat, J., Garcia, M.A., Cruzado, A., Palanques, A., Arín, L., Gomis, D., Guillen, J., de León, A., Puigdefàbregas, J., Sospedra, J., and Velásquez, Z.R.: Seasonal changes of water mass structure and shelf-slope exchanges at the Ebro Shelf (NW Mediterranean), Continental Shelf Research 22 (2002), 327-348, 2002.

Schmidt, R.: Multiple emitter location and signal parameter estimation, IEEE Trans. Antennas Propag., 34, pp. 276-280, 1986.

~~Shay, L.K., Cook, T.M., Peters, H., Mariano, A.J., Weisberg, R., Edgar An, P., Soloviev, A., and Luther, M.: Very High Frequency radar mapping of surface currents, IEEE Journal of Oceanic Engineering, Vol. 27, NO. 2, April, 2002.~~

Solabarrieta, L., Rubio, A., Castanedo, S., Medina, R., Charria, G. and Hernández, C.: Surface water circulation patterns in the southeastern Bay of Biscay: New evidences from HF radar data, Continental Shelf Research 74, pp. 60–76, 2014.

Sotillo, M.G., Cailleau, S., Lorente, P., Levier, B., Aznar, R., Reffray, G., Amo-Baladrón, A., and Alvarez-Fanjul, E.: The MyOcean IBI Ocean Forecast and Reanalysis Systems: Operational products and roadmap to the future Copernicus Service, Journal of Operational Oceanography, pp. 1-18, 2015.

Stanev, E.V., Ziemer, F., Schultz-Stellenfleth, J., Seemann, J., Staneva, J. and Gurgel, K.W.: Blending Surface Currents from HF Radar Observations and Numerical Modelling: Tidal Hindcasts and Forecasts, Journal of Atmospheric and Oceanic Technology, Vol. 32, pp. 256-281, 2015.

Taylor, K.E.: Summarizing multiple aspects of model performance in a single diagram, Journal of Geophysical research, 106, pp. 7183-7192, 2001.

Trujillo, D.A., Kelly, F.J., Perez, J.C., Riddles, H.R. and Bonner, J.S.: Accuracy of Surface Current Velocity Measurements Obtained from HF Radar in Corpus Christi Bay, Texas, IEEE/ IGARSS Geoscience and Remote Sensing Symposium, 2: 1179–1182, 2004.

Wyatt, L.: Improving the quality control and accuracy of HF radar currents, IEEE Oceans 2015, Genova, pp 1-9, 2015.

Yoshikawa, Y., Masuda, A., Marubayashi, K., Ishibashi, M., and Okuno, A.: On the accuracy of HF radar measurement in the Tsushima strait, Journal of Geophysical Research, 111, doi:10.1029/2005JC003232, 2006.

Con formato: Normal, Justificado, Punto de tabulación: No en 0,75 cm

SITE STATUS		
Type	**Parameter**	**Description**
Receiver	MTMP, RTMP	Chassis and board temperatures.
Transmitter	XPHT, XAHT	Chassis and amplifier temperatures.
Transmitter	XAFW, XARW	Forward and reflected powers.
Antenna	SNR1, SNR2, SNR3	Signal-to-Noise ratio at loop 1, loop 2 and the monopole.
Antenna	AMP1, AMP2	Calculated amplitude corrections for loops 1 and 2 to the monopole.
Radial	Number radials / u.t,	Abrupt decrease can be related to a potential

	Range and bearing	malfunction
SYSTEM STATUS		
Parameter		**Description**
Temporal coverage		Data availability (%): areas of poor data return (<50%) are discarded from any analysis.
Evolution of spatial coverage		Monitoring of fluctuations due to day/night cycle. Identification of time-steps of sharp decrease in spatial coverage.
Spatial coverage–VS–Temporal coverage		Verification of the 80%-80% recommended level of data provision.
COS uncertainty metrics (standard deviation of U/V, covariance U/V)		Useful resource, based on fluctuations in the data themselves.

Table 1. Diagnose parameters used to operationally monitor Ebro Delta HF radar status in real time. The HF radar system's performance is routinely evaluated through the analysis of the aforelisted indicators on different frequencies (daily / weekly / monthly).

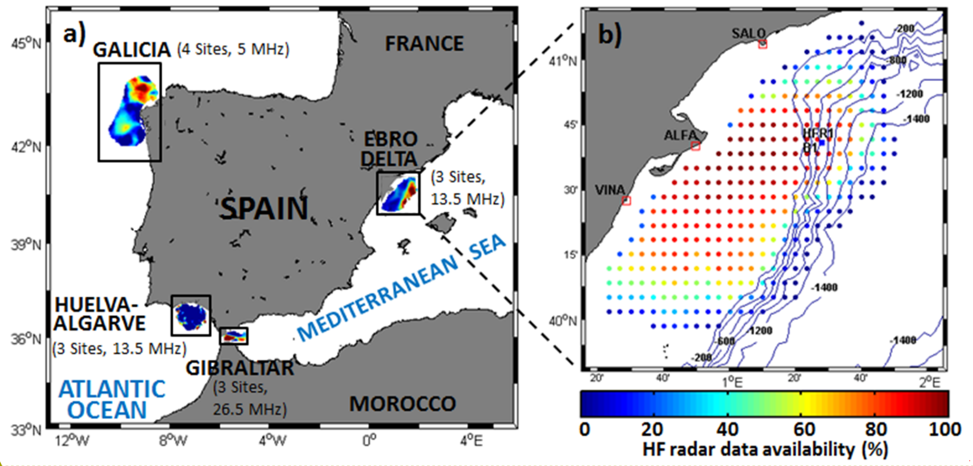

Con formato: Fuente: 11 pto, Negrita

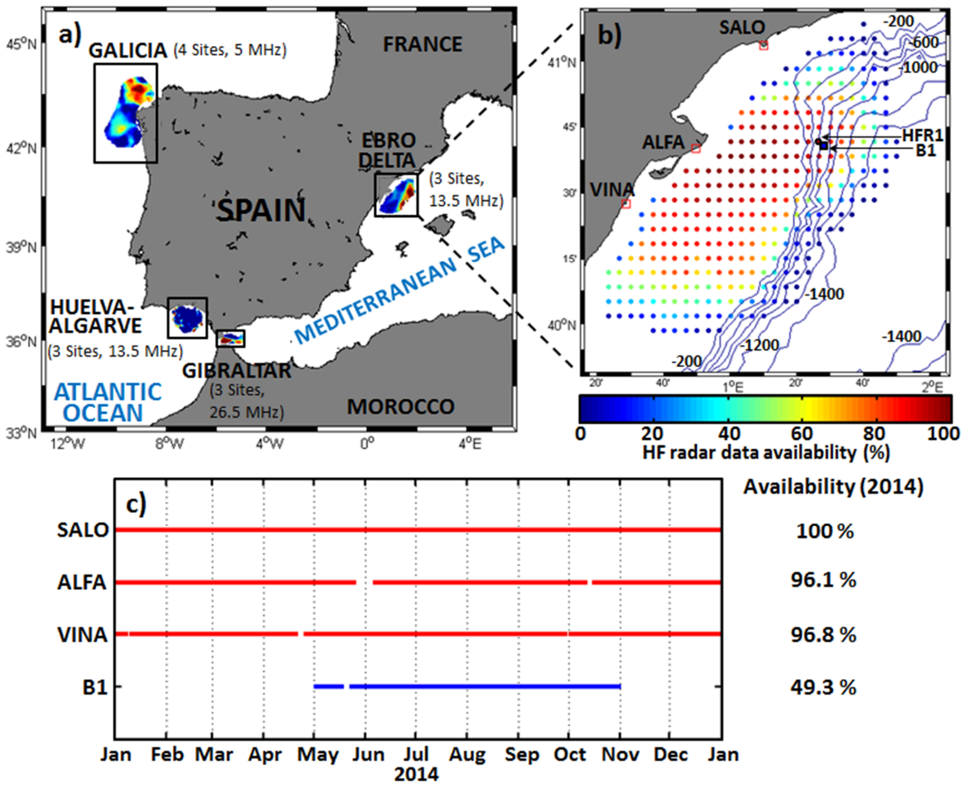

Figure 1. (a) HF coastal radar network currently operated by Puertos del Estado (b) HF radar deployed at the Ebro Delta, composed by three sites: Salou (SALO), Alfacada (ALFA) and Vinaroz (VINA). Colored dots denote the temporal coverage in percent of HF radar surface current total vectors for the entire year 2014. Isobath depths are labeled every 200 m. Location of Tarragona buoy (B1) is marked with filled blue squares. HFR1 denotes the radar grid point closest to B1 position. . (c) Time lines of HF radar sites (red) and B1 buoy (blue) current data availability for 2014.

Con formato: Fuente: 11 pto, Negrita

1 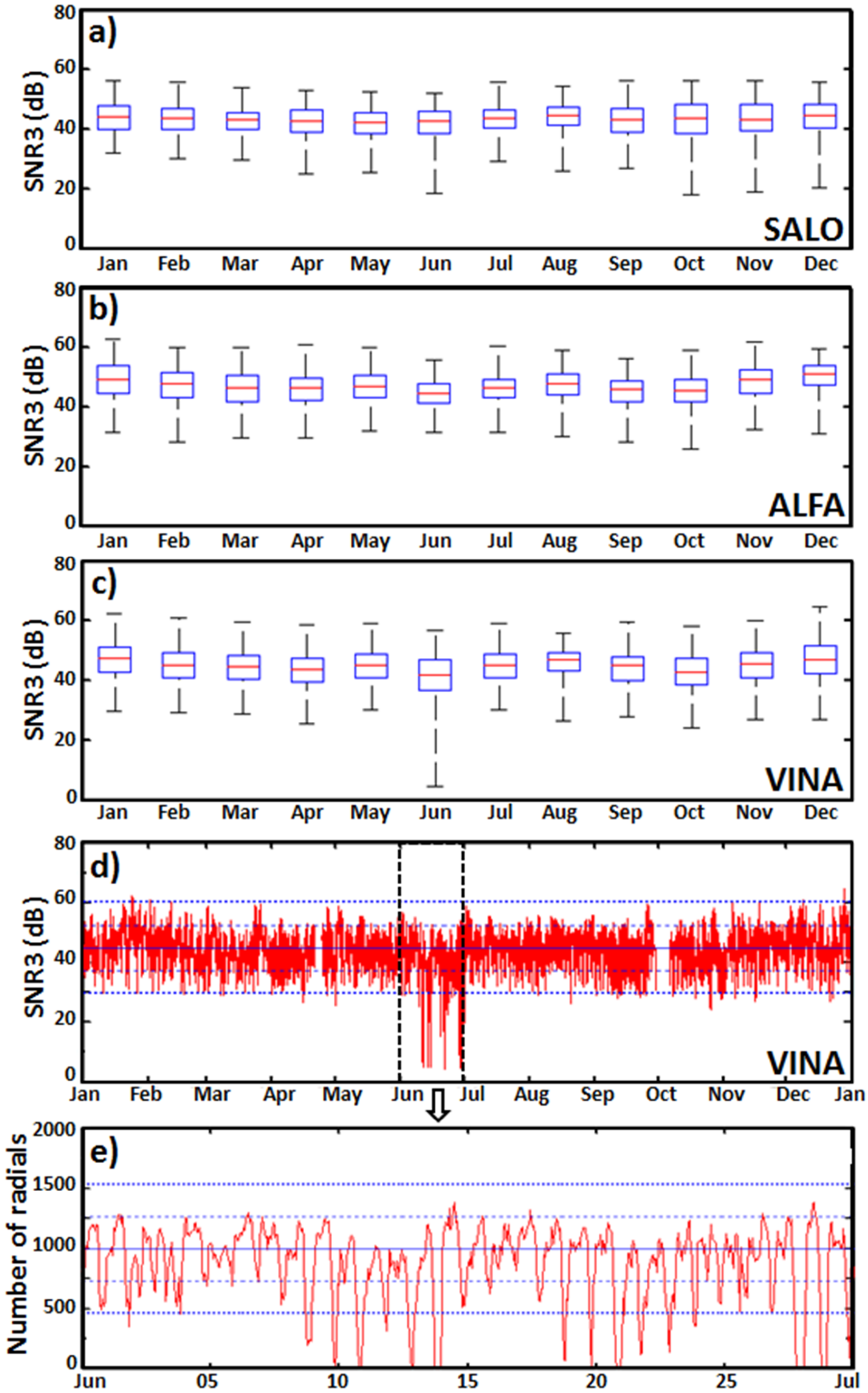
a)
b)
c)
d)
e)
SNR3 (dB)
Number of radials
SALO
ALFA
VINA
VINA
Jan Feb Mar Apr May Jun Jul Aug Sep Oct Nov Dec
Jun 05 10 15 20 25 Jul

Figure 2. Annual quality control of Ebro Delta radar sites, SALO (a), ALFA (b) and VINA (c), based on monthly boxplots of Signal-to-Noise Ratio at the monopole (SNR3) for 2014. On each box, the central mark is the median, the edges of the box are the 25th and 75th percentiles, and the whiskers extend to the most extreme data points. ~~An abrupt decrease (below 10 dB) is observed in VINA in June. The annual time serie of hourly SNR3 values for VINA site (d) reveals that the imposed thresholds of two standard deviations above/below the mean (bold blue dotted lines) are exceeded several times along June, reaching extremely low values which are related to a lower number of radial vectors provided by VINA site (e). The solid and dashed blue lines represent the mean and the standard deviation for the entire 2014, respectively.~~

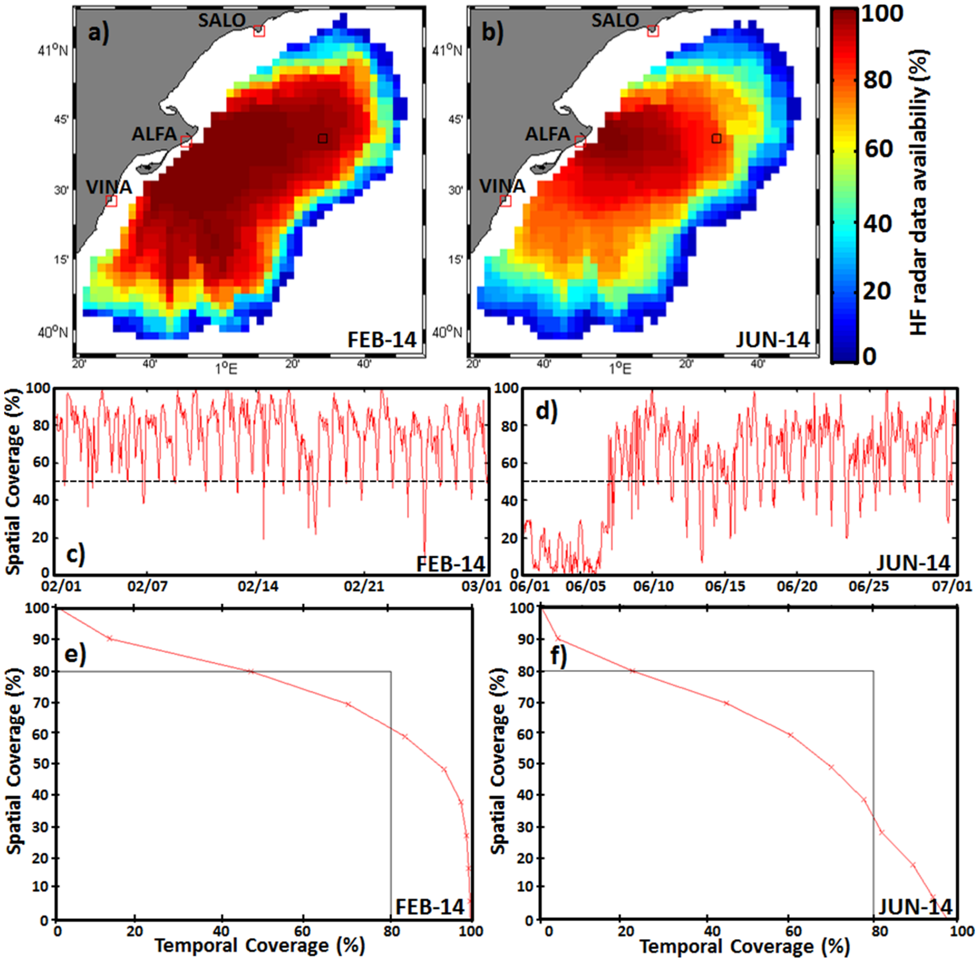

Figure 3. Evaluation of Ebro Delta HF radar system performance on a monthly basis: February (left) and June (right), 2014. A comparative analysis is carried out for the radar data availability (a-b), the temporal evolution of the spatial coverage (c-d) and the relationship between both the spatial and temporal coverage (e-f). The black square represented in (a-b) denotes B1 buoy location.

1 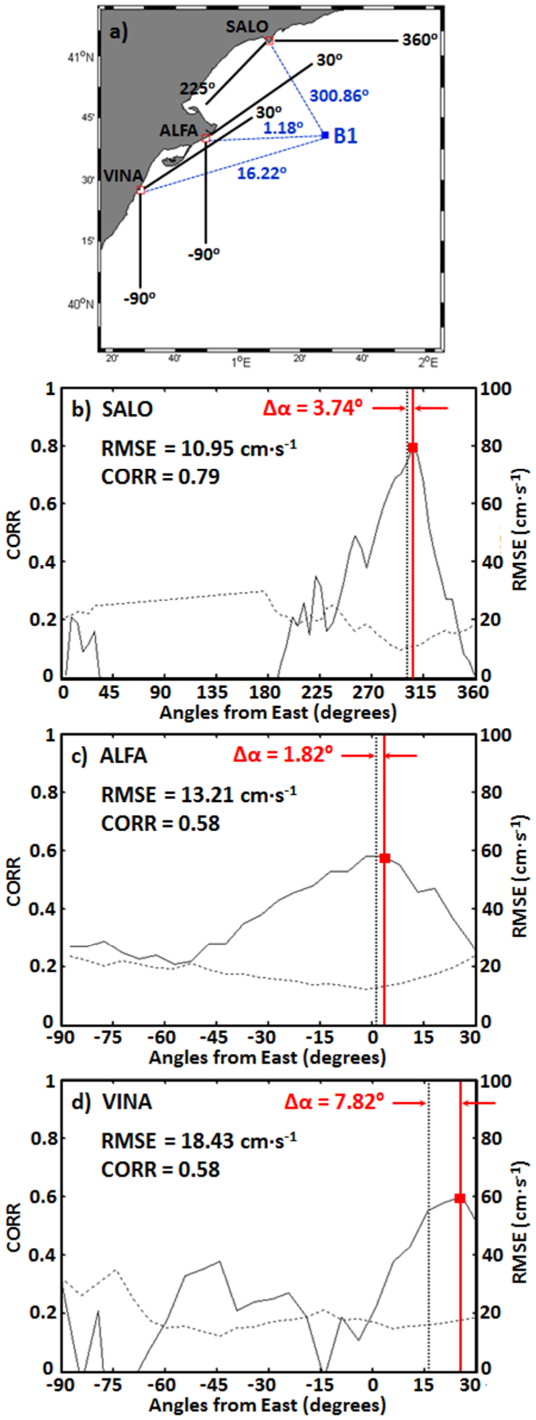
a)
SALO
360°
41°N
30°
225°
300.86°
45'
30°
ALFA
1.18°
B1
30'
VINA
16.22°
15'
-90°
-90°
40°N
20'
40'
1°E
20'
40'
2°E
b) SALO
Δα = 3.74°
RMSE = 10.95 cm·s-1
CORR = 0.79
CORR
RMSE (cm·s-1)
Angles from East (degrees)
c) ALFA
Δα = 1.82°
RMSE = 13.21 cm·s-1
CORR = 0.58
d) VINA
Δα = 7.82°
RMSE = 18.43 cm·s-1
CORR = 0.58

Figure 4. (a) Angular position of Ebro Delta HF radar sites respect to B1 buoy location. Angle values are measured counter-clockwise from East, indicating arc limits and buoy direction. (b-d) Correlation (solid line) and RMSE (dashed line) between unfiltered radial currents estimated by B1 buoy and those measured by three HF radar sites, SALO (b), ALFA (c), and VINA (d), using calibrated antenna patterns for a 6-month period May-October 2014. Vertical dotted line represents the angular position of B1. Vertical red solid line denotes the angular position of maximum correlation (CORR), which is gathered with the associated RMSE and bearing offset ($\Delta\alpha$) values.

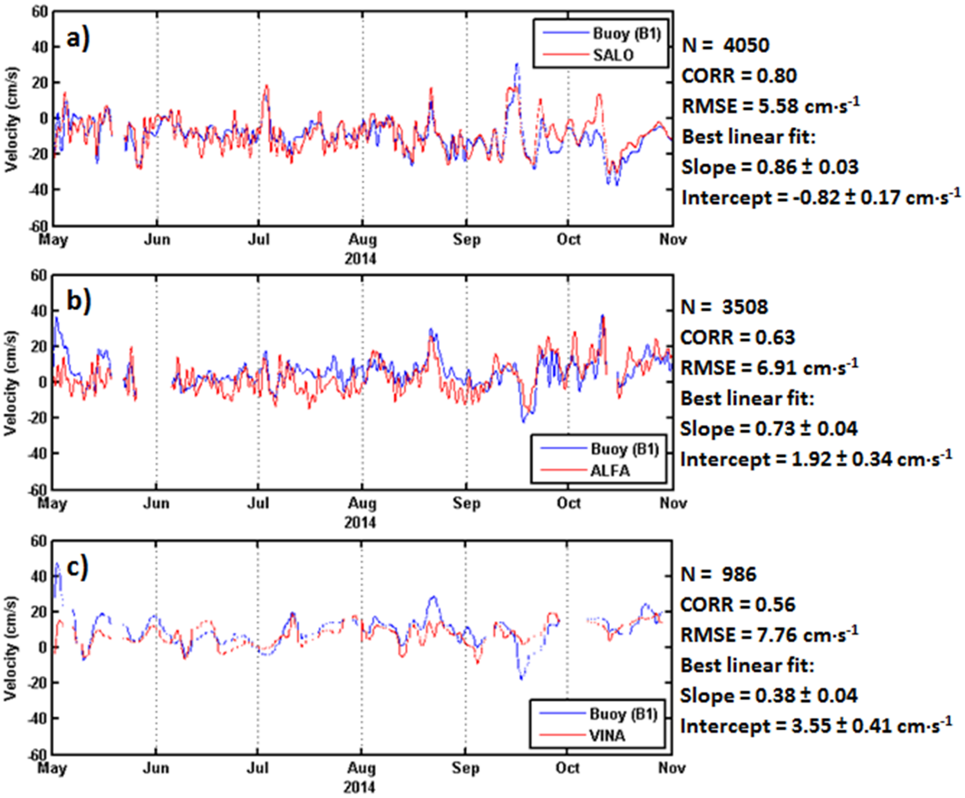

Figure 5. Comparison of low-pass filtered hourly time series (cut-off period of 30 h) of radial currents measured by B1 buoy (blue line) and HF radar sites (red lines): (a) SALO, (b) ALFA and (c) VINA in the range arc point closest to B1 location for a 6-month period May-October 2014, using calibrated antenna patterns. N, slope and intercept represent the number of hourly radial current observations and the results derived from the best linear fits, respectively.

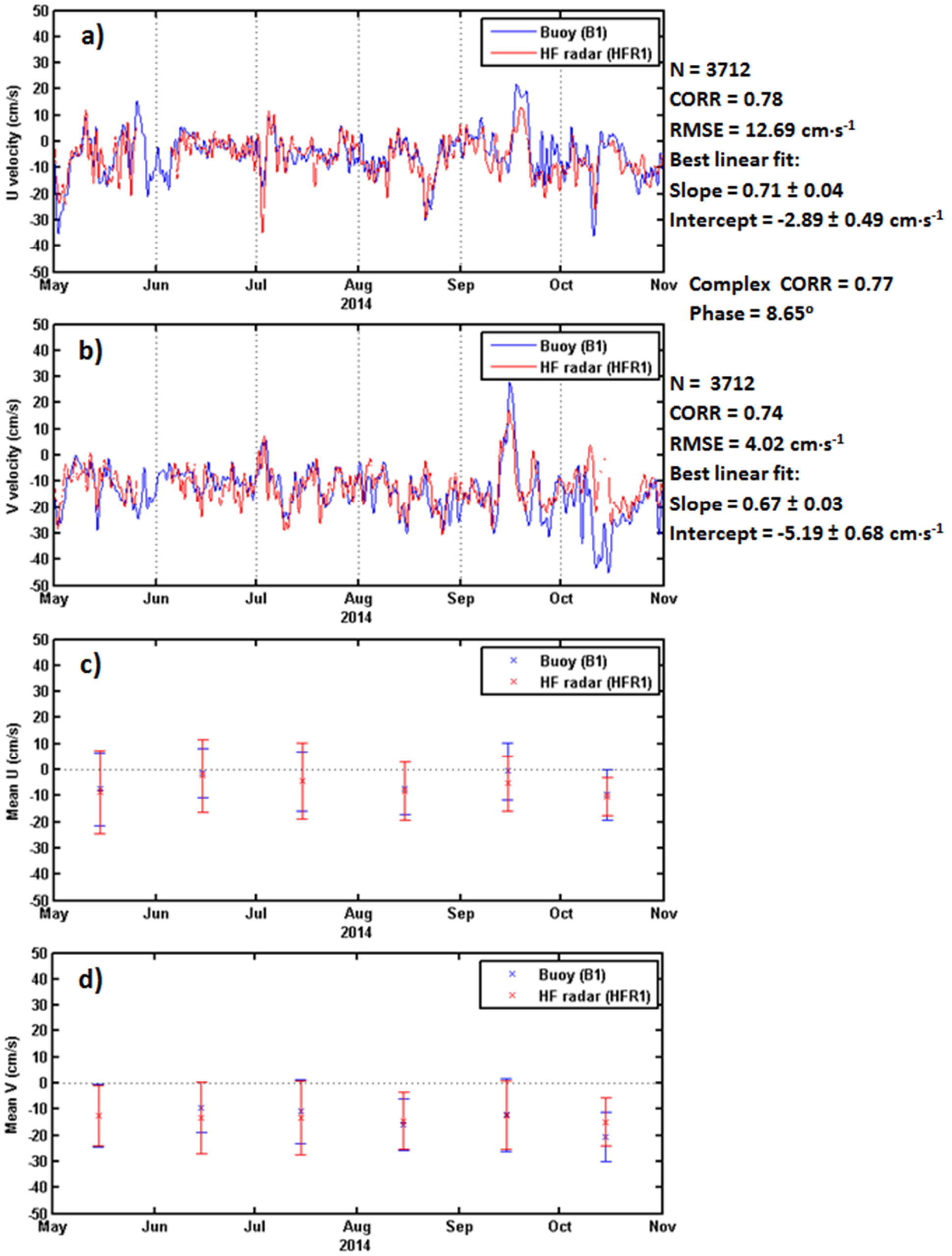
a)
Buoy (B1)
HF radar (HFR1)
U velocity (cm/s)
N = 3712
CORR = 0.78
RMSE = 12.69 cm·s-1
Best linear fit:
Slope = 0.71 ± 0.04
Intercept = -2.89 ± 0.49 cm·s-1
Complex CORR = 0.77
Phase = 8.65º
b)
V velocity (cm/s)
N = 3712
CORR = 0.74
RMSE = 4.02 cm·s-1
Best linear fit:
Slope = 0.67 ± 0.03
Intercept = -5.19 ± 0.68 cm·s-1
c)
Mean U (cm/s)
d)
Mean V (cm/s)
May
Jun
Jul
Aug
Sep
Oct
Nov
2014

Figure 6. Low-pass filtered (cut-off period of 30 h) hourly time series of zonal (a) and meridional (b) components of total currents measured by B1 buoy (blue line) and HF radar at the closest grid point HFR1 (red line), for a 6-month period May-October 2014. Mean zonal (c) and meridional (d) current velocities, averaged over individual months for both HF radar and B1 measurements, with one standard deviation (error bars represent the 95% confidence interval).

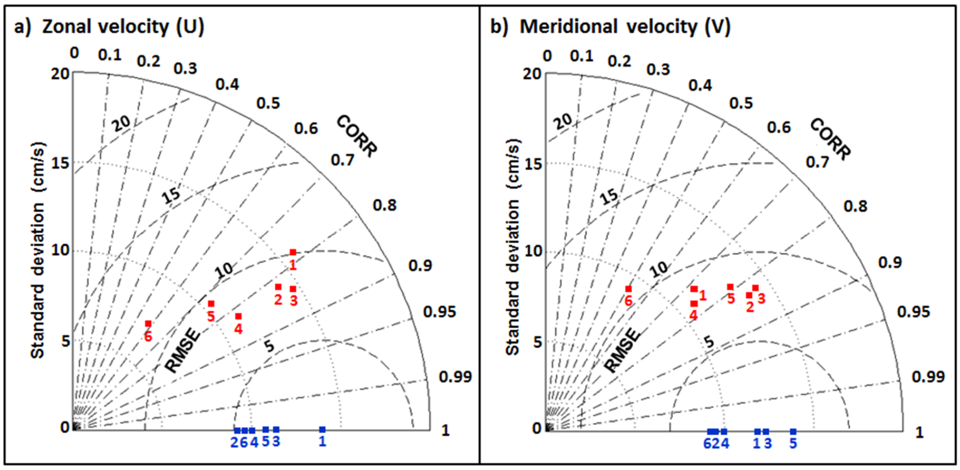

Figure 7. Taylor diagrams, based on the law of cosines, provide a concise statistical summary of how closely unfiltered hourly radar estimations (red filled squares) match with B1 observations (blue filled squares), considered here as the reference points of perfect agreement. Taylor diagrams for zonal (a) and meridional (b) velocity components gather the monthly statistical metrics derived from HF radar – B1 comparison. Sequential numbers refer to individual months of the analyzed period May-October 2014 (1: May; 6: October).

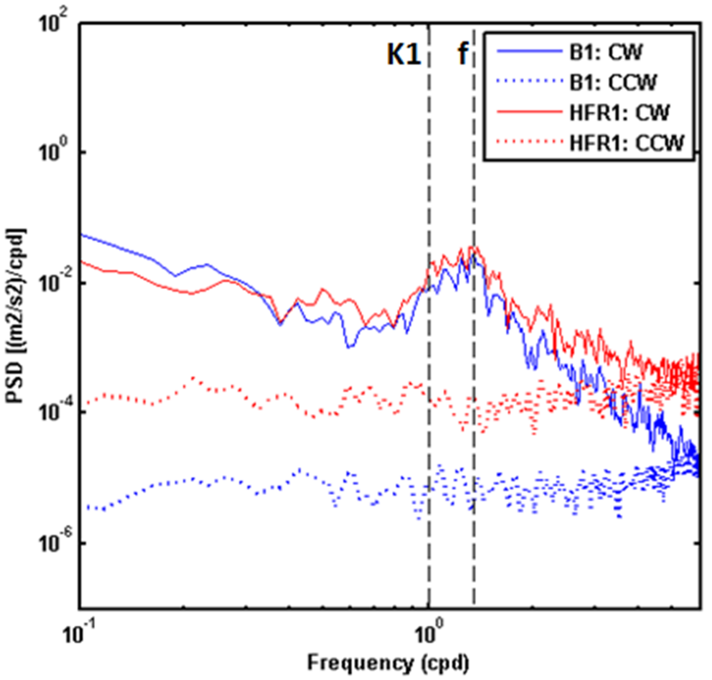

Con formato: Fuente: 12 pto

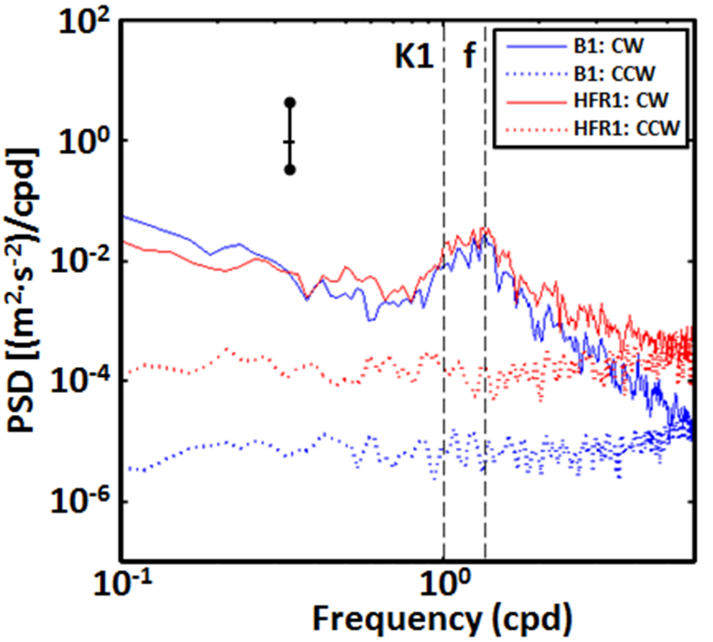

Figure 8. Spectral density of the rotary auto-spectra of B1 buoy (blue) and HF radar at the closest grid point HFR1 (red), performed for a 6-month period May-October 2014 of concurrent records. Clockwise (counter-clockwise) components are represented by solid (dotted) lines. Vertical dashed lines indicate the frequencies of the diurnal constituent (K_1) and the inertial oscillations (f). Error bars indicate the 95% confidence interval.

Con formato: Fuente: 12 pto, Negrita

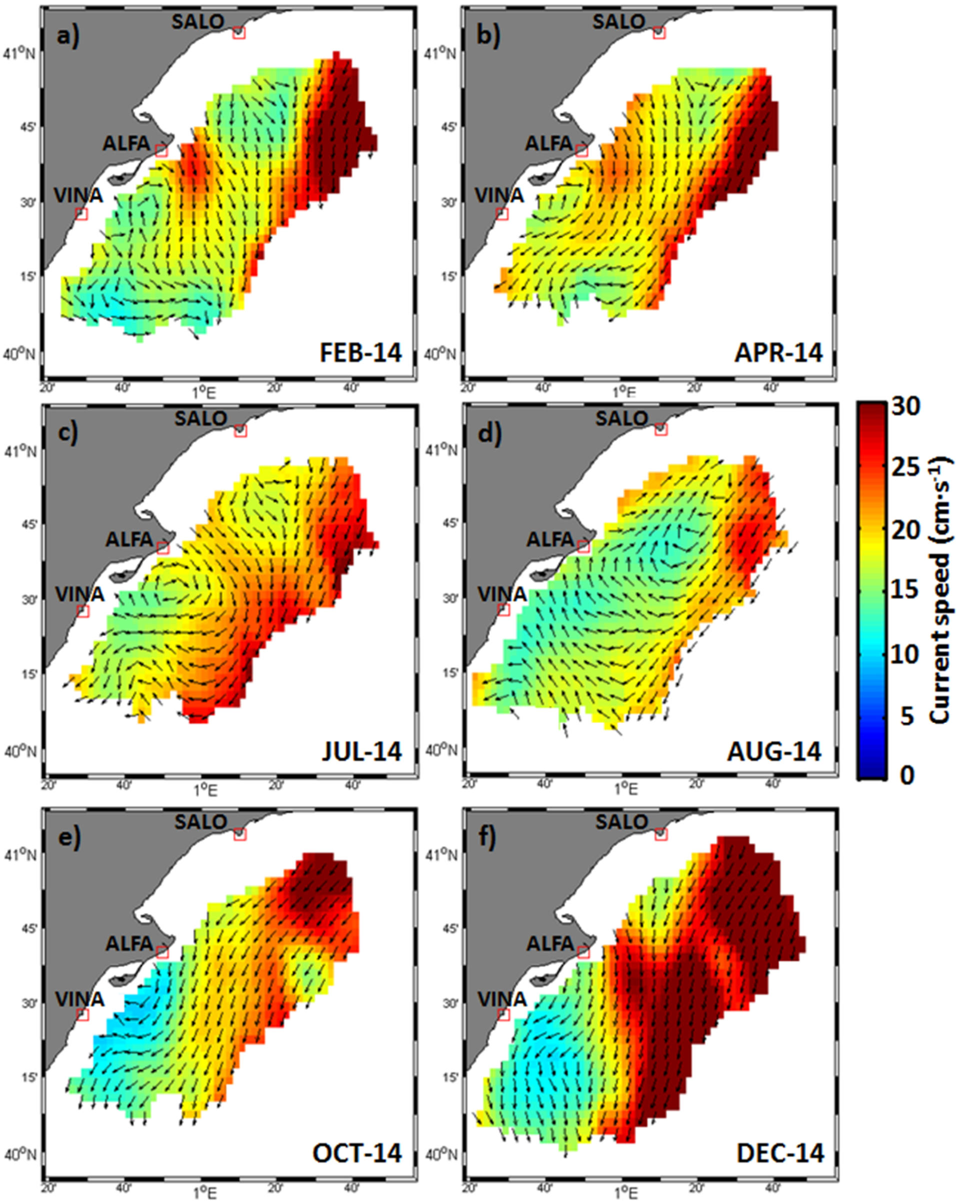

Figure 9. Monthly averaged surface velocity fields, based on unfiltered hourly HF radar current data, for (a) February, (b) April, (c) July, (d) August, (e) October, and (f) December

2014. The study area is not uniformly covered since only radar grid points satisfying a minimum data return of 50% over the monthly record have been considered. Only one grid point of every two is plotted for visualization reasons. Only one grid point of every two is plotted for visualization reasons.

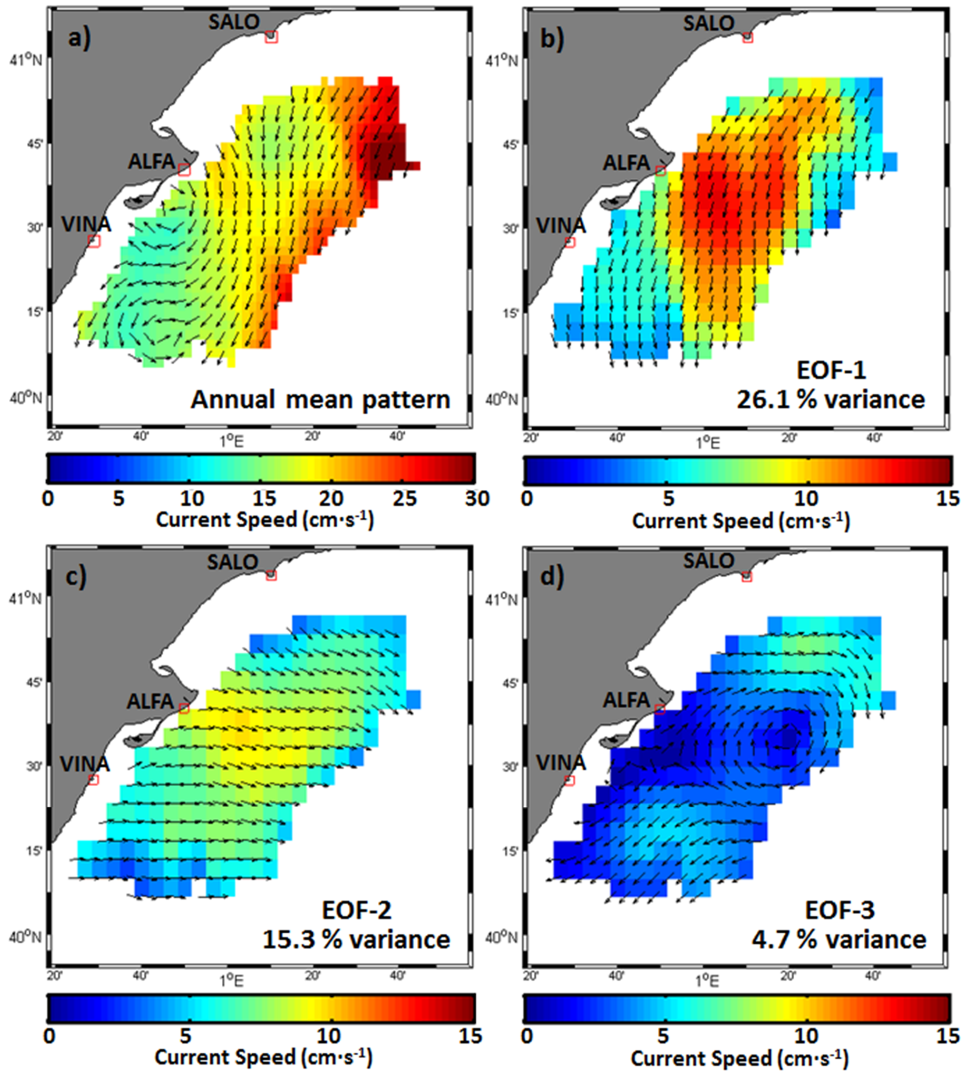

Figure 10. Spatial patterns of the (a) annual mean velocity field and (b) first, (c) second and (d) third EOF dominant modes of unfiltered hourly radar surface currents for 2014. Current vectors were plotted in every second grid point for clarity. Variance explained is indicated in the lower right corner of the corresponding panel.

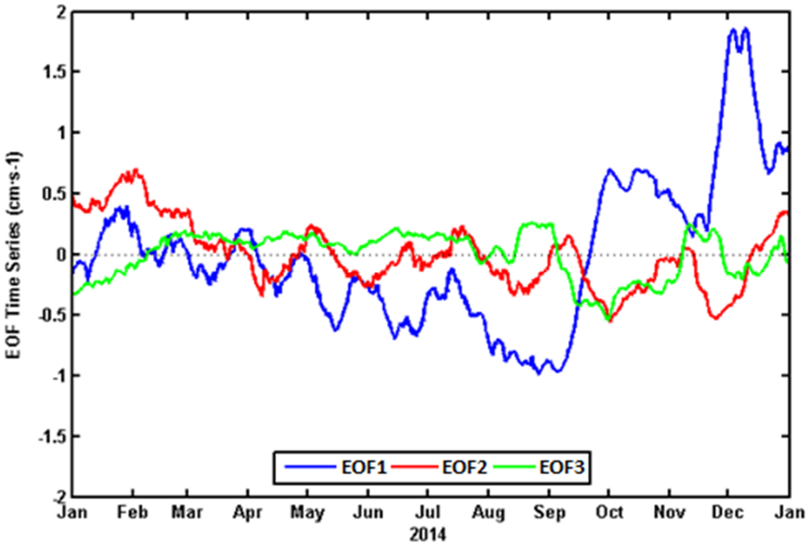

Figure 11. Time coefficients of the first (blue), second (red) and third (green) EOF modes of hourly radar current data set evaluated for the entire year 2014. Time series have been filtered with a 20 day running mean.

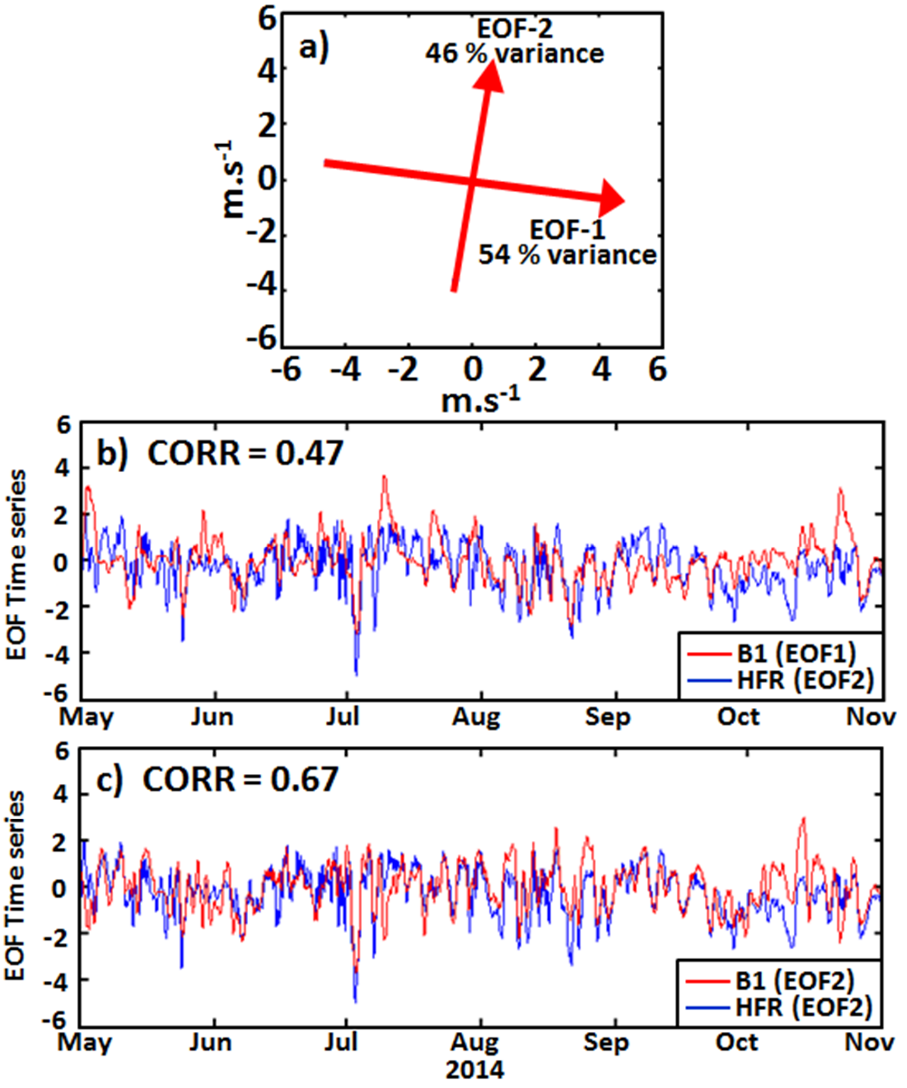

Figure 12. (a) Main axes of variability for hourly wind data registered at B1 buoy. (b) Principal components of the first EOF mode of wind (m/s, in red) and the second EOF mode of radar currents (cm/s, in blue). (c) Principal components of the second EOF mode of wind (red) and the second EOF mode of radar currents (blue). The amplitudes have been normalized by their respective standard deviations and filtered with a 1 day running mean.

Con formato: Fuente: 12 pto